University of Twente

Jasper Ringoot

Daily supervisor: Dr. Cees Otto
Committee member: Prof. Dr. Leon Terstappen
External member: Prof. Dr. Armağan Koçer
External member: Dr. Ir. Nienke Bosschaart

Creation and validation of a 405 nm laser Raman imaging setup

October 27, 2022

Contents

1 Introduction and Raman theory **3**
- 1.1 Raman Spectroscopy . . . 4
- 1.2 Integration Raman spectroscopy - microscopy . . . 5
- 1.3 Different excitation wavelengths . . . 6
- 1.4 Applications Raman . . . 7
- 1.5 Blue light (405nm) laser setup . . . 8

2 405nm Raman Setup, method and results **9**
- 2.1 Overview . . . 9
- 2.2 Laser . . . 10
  - 2.2.1 Method . . . 10
  - 2.2.2 Results . . . 11
    - 2.2.2.1 Optical fiber stability . . . 11
    - 2.2.2.2 Power output and input . . . 12
- 2.3 Shutter & trigger . . . 13
- 2.4 Laser cleanup filter . . . 14
- 2.5 Polariser . . . 16
- 2.6 Beam expander . . . 16
- 2.7 407nm razor edge filter . . . 17
- 2.8 XYZ stage . . . 19
- 2.9 Objective . . . 19
- 2.10 40x40 μm stage . . . 20
- 2.11 Blue transmission light LED . . . 21
  - 2.11.1 Blue light cover slide . . . 21
- 2.12 Slide holder . . . 23
- 2.13 Polarisation filters . . . 23
- 2.14 CCD camera . . . 24
- 2.15 Fidgets . . . 26
  - 2.15.1 ND filters . . . 26
  - 2.15.2 50/50 beamsplitter . . . 26
- 2.16 Blue LED calibration light . . . 27
- 2.17 Krypton lamp . . . 27
- 2.18 405 nm long pass razor edge . . . 29
- 2.19 Prism box . . . 30
- 2.20 Pinhole focus lens . . . 31
- 2.21 Spectroscope . . . 31

3 Method calibration and cells **33**
- 3.1 Toluene measurements . . . 33
- 3.2 Red Blood Cells . . . 33
- 3.3 White Blood Cells donor . . . 33

3.4 QCR program analysis . . . 34
3.5 Principle Component Analysis (PCA) . . . 35

4 Results calibration and cells **36**
4.1 Toluene . . . 36
4.2 Red Blood Cells . . . 37
4.2.1 First RBC . . . 37
4.2.2 Laser inflicted cell damage . . . 38
4.2.3 Signal regression . . . 38
4.2.4 Oxygenation state . . . 43
4.3 White Blood Cells . . . 44
4.3.1 Cultured THP-1 cells . . . 44
4.3.2 Donor sample WBCs . . . 47
4.4 Other applications . . . 50
4.4.1 Crystal detection inside synovial fluid . . . 50

5 Discussion **53**
5.1 Setup . . . 53
5.1.1 Laser . . . 54
5.1.2 Beam expander . . . 54
5.1.3 XYZ stage . . . 54
5.1.4 Polarisation filters . . . 54
5.1.5 CCD camera . . . 55
5.1.6 Pinhole focus lens . . . 55
5.2 Cells and other objects . . . 55
5.2.1 RBC . . . 55
5.2.2 WBC . . . 55
5.2.3 THP-1 . . . 55
5.2.4 Donor sample WBC . . . 55
5.2.5 Other applications . . . 56

6 Conclusion **57**
6.1 405 nm setup . . . 57
6.2 Experiments . . . 57

7 Acknowledgements **58**

A Appendix **59**
A.1 Matlab script for asc file analysis . . . 61
A.2 Matlab script for spectroscope calibration file analysis . . . 63

1 Introduction and Raman theory

On the 28 February 1928, Indian physicist Chandrasekhara Venkata Raman and his assistant Kariamanikkam Srinivasa Krishnan, discovered a light scattering effect which is known today as the phenomenon of Raman scattering. Raman received a Nobel prize in physics for his discovery in 1930. Raman spectroscopy (the detection of Raman scattering at different wavelengths of light) has its use in many scientific fields including chemistry, solid-state physics, biology and medicine. In the field of cell biology, it is often of great use to specifically know which enzymes and molecules are present in a cell. Disease diagnosis, measuring the uptake of a cell or identifying foreign chemicals and molecules are all possible applications of Raman spectroscopy. This master thesis will focus on the creation and validation of a novel 405 nm Raman spectroscopy microscope to identify enzymes in white blood cells. This setup uses the principle of resonant Raman (RR) to scan different samples for their content.
This thesis consists of several components: The building of the 405nm setup, the validation of this setup to measure Raman signal and the measurements on different cell types to identify enzymes. Chapter 1.1 will cover how a (Resonant) Raman signal is created and used, what the history of this technique is regarding to enzyme identification and why this setup is made in the first place. After chapter 1.1, the design of the 405nm setup will be discussed in chapter 2, covering the individual components and their validation. This validation will be continued with chapter 4 where the setup is used to measure both red blood cells (RBC) and white blood cells (WBC).

1.1 Raman Spectroscopy

Raman spectroscopy relies on the principle of inelastic scattering photons, also known as Raman scattering. Energy from incoming photons will change the vibrational state of a molecule and redistribute its electrons. A vibrational state change will be Raman active when the polarisation changes during vibration. Raman scattering is similar in a few ways to fluorescent emission, but also has distinctive properties which make it unique. Figure 1 shows the difference between fluorescent emission, nonresonant Raman (nRR) scattering and resonant Raman (RR) scattering. Vertical arrows represent photon fields. Horizontal lines represent the vibrational energy level states (v_x) of the material (encompassing the distribution of electrons and nuclei). The photon field causes transition between different vibrational states of a molecule. With fluorescent emission a photon is absorbed, causing a change of the vibrational state of the molecule where the electrons are distributed from the ground state to a higher excitation band. Here it relaxes to the lowest excited state and afterwards falls back to a ground vibrational energy level, emitting a photon in the process. Fluorescent emission is only possible when fluorophores are present inside a sample. Raman scattering always is a two-photon process where a molecule only spends a very short time (femto-second scale) in a higher vibrational state. Fluorescent emission takes relatively longer (nano-second scale). A molecule's ability to change polarisation during a vibration change is dependent on its polarisability. Raman polarisability α is described with equation 1.

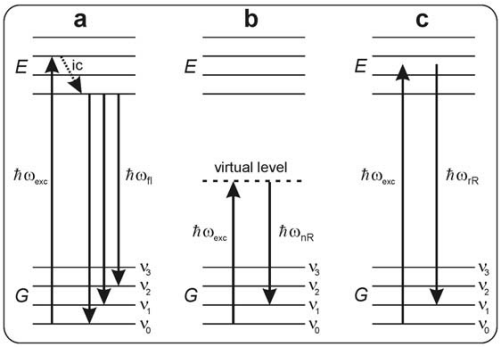

Figure 1: Energy level diagrams for fluorescent emission (a), nonresonant Raman scattering (b), and resonant Raman scattering (c). Upwards arrows indicate electron excitation; downwards arrows indicate electrons falling back to ground state.[1]

$$\overleftrightarrow{\alpha} = \sum_j \left\{ \frac{A}{\hbar(\omega_{ji} - \omega_L) - i\Gamma_{ji}} \right\} \tag{1}$$

A is the amplitude of a vibrational transition dipole moment, $\hbar$ is Planck's constant, ω_{ji} is the frequency of a molecule's absorption band, ω_L is the frequency of the excitation laser and Γ_{ji} is the damping. The difference between non resonant Raman and resonant Raman lies in the distance between ω_{ji} and ω_L. When the excitation laser frequency lies closer to the frequency of the absorption band the denominator becomes smaller and the polarisability increases. With resonance Raman these frequencies lie closer together and will generate more signal compared to non resonant Raman where the frequencies are further apart.

1.2 Integration Raman spectroscopy - microscopy

The small red shift in the spectrum of light is the chemical characterisation principle of Raman spectroscopy. The amount of red shift depends on the individual molecule or chemical bond and which vibrational modes it possesses. Falling back to a lower vibrational level will result in a small Raman shift; the difference in energy and thus wavelength is relatively small. When an electron falls back to a higher vibrational level, the difference between the excitation and emission is larger, making the Raman shift larger as well. Raman shift is expressed in cm^{-1} and is often displayed on the x-axis, with the counts or intensity on the y-axis. Every molecule, atom and chemical bond has its own unique Raman spectrum. Distinctive peaks at specific Raman shifts make a spectrum unique. Figure 2 shows the Raman spectrum of haemoglobin. The most prominent peaks are indicated with their respective Raman shift.

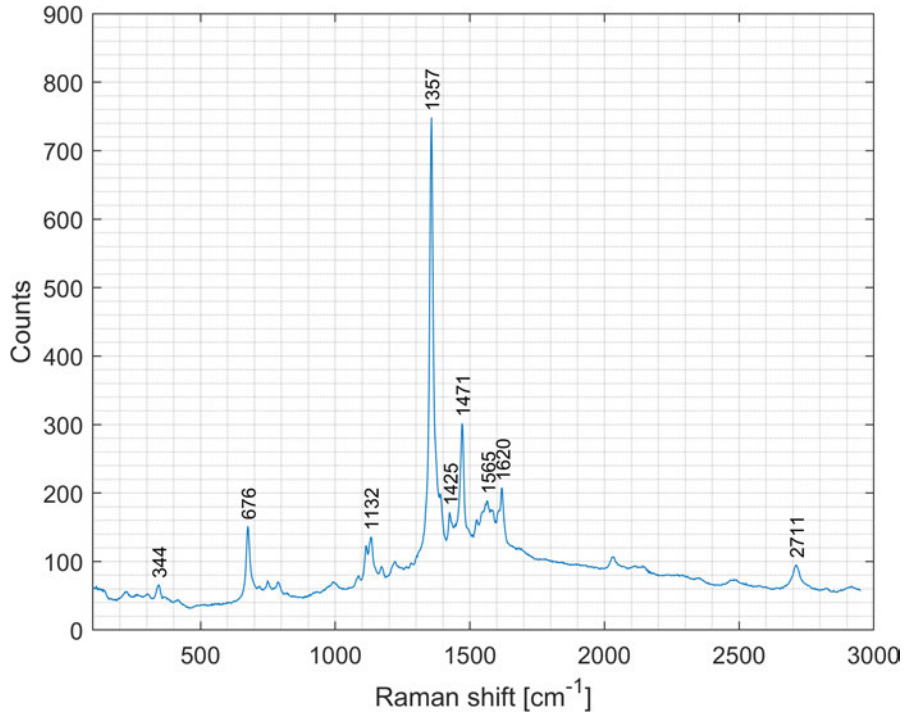

Figure 2: Haemoglobin spectrum from 100 cm^{-1} to 2950 cm^{-1}. 405nm, 195 μW, 100ms exposure time, average of 9 pixels.

This spectral output can now be combined with microscopy. Shining the excitation and emission light through an objective makes it possible to analyse Raman signal at a small scale. Adding a movable XYZ-stage enables the option to make 2D and 3D confocal scans of a surface. Giving each pixel its own distinct Raman spectrum and making identification of different materials possible.

1.3 Different excitation wavelengths

Raman setups are able to work with different wavelengths/colours of laser light. The advantage of the Raman shift is that it is independent of the wavelength used. When one measures a red blood cell with a 405nm and 647nm laser for instance, both results will indicate the positions of the peaks as given in figure 2. The major difference between the two would be the ratio in the height of the peaks and the Raman scattering cross section. Raman scattering increases when the laser excitation wavelength approaches a transition wavelength in a molecule, as seen in equation 1.
Molecules are sensitive to specific wavelengths of excitation light which depends on their absorption spectrum. The absorption spectrum shows the transition dipole moments in a molecule. Figure 3 shows the absorption spectrum of oxygenated and deoxygenated haemoglobin. Around 400nm a high absorbance area called the Soret band is present. Matching an excitation wavelength to this area, like a 405nm laser, theoretically yields a high signal output. The Soret bands for haemoglobin and oxyhaemoglobin have slightly different peak locations. Around 410 nm for oxyhaemoglobin and around 440 nm for haemoglobin. Comparing their polarisability with equation 1 shows $\omega_{ji} - \omega_L = 440 - 405 = 35$ for heamoglobin and $\omega_{ji} - \omega_L = 410 - 405 = 5$ for oxyhaemoglobin. Giving a factor 7 difference between the two. Meaning oxyhaemoglobin's polarisability is 7 times higher than that of haemoglobin.

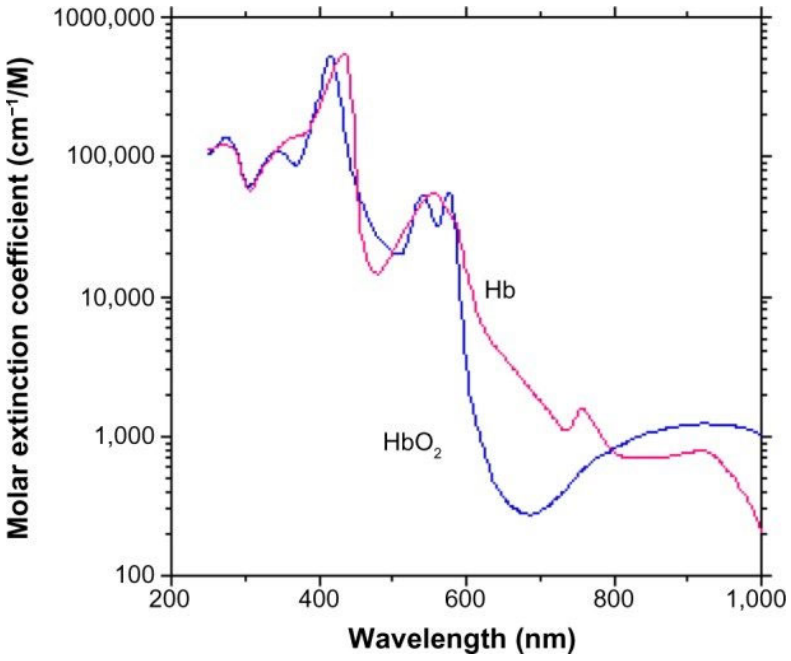

Figure 3: Haemoglobin absorption spectrum from *Nitzin et al.*[2] Note the logarithmic scale on the y-axis.

1.4 Applications Raman

Raman has been used over the past few decades to identify all sorts of molecules and chemicals.[3–6] Here the scope is constrained to research in enzyme detection in both red and white blood cells. One important factor is the porphyrin molecule. Porphyrin is a component of haem, which in turn is a precursor to haemoglobin and myeloperoxidase (MPO). Which are important molecules in respectively red and white blood cells. A typical absorption spectrum of porphyrin, as shown in figure 4, is well suited for detection by Resonant Raman spectroscopy. On the left side of the spectrum the typical Soret band can be seen.[7] This Soret band is a high absorbance region around 400nm and while absorption competes with the RR signal, it still enables significantly more signal compared to nRR imaging of porphyrin molecules.

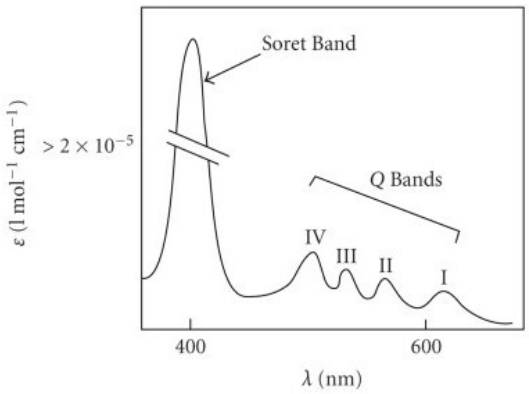

Figure 4: Typical absorption spectrum porphyrin.[8]

Earlier research has already shown the possibilities in detecting enzymes with both RR and nRR. In 2003 *Van Manen et al.*[9] have shown that, with a laser at 413nm, they were able to obtain cytoplasmic spectra of single neutrophils. Locating enzymes in the 1375 cm^{-1} band and the location of polystyrene (PS) particles in the same neutrophil. Three years later in 2006, *Van Manen et al.*[1] compared the differences between measuring NADPH oxidase with RR and nRR within single neutrophils that had PS particles inside. *Krafft et al.*[10] showed the possibility to image single organelles with nRR in 2007. *Vanna et al.*[5] used the home-built 647nm laser setup to distinguish different typical cells that were diagnosed with acute myeloid leukaemia (AML) and myelodysplastic syndrome (MDS). More recently (2020) *Dorosz et al.*[6] showed the measurement of EPO and MPO (in eosinophils and neutrophils) using three different excitation wavelengths: 532nm, 633nm and 785nm.

1.5 Blue light (405nm) laser setup

As mentioned in section 1.4, most studies used nRR with only a few using RR.
nRR setups are able to measure individual enzymes, but come with several disadvantages. nRR spectra are often obtained using high laser powers ($\sim$ 10-35mW) and long exposure times per pixel (several seconds to minutes). When trying to scan an entire cell with the pixel resolution close to the diffraction limit of light ($\sim \lambda/2$), the total measurement time per cell quickly rises to tens of minutes and even hours when the exposure time per pixel is longer. As explained at the beginning of section 1.1, each molecule has its own absorption spectrum. Exciting with a laser frequency that lies further from the absorption band frequency results in less polarisability and less signal. Using nRR the polarisability will be low for most molecules, meaning no single molecule will jump out due to a very high polarisability and thus high signal. With the strong absorption bands that are the Soret bands it makes sense to use a RR laser close to the peak of the bands. Increasing the polarisability and detectability of these molecules. The 405 nm laser lies close to the Soret peaks, making it a suitable choice for a RR setup.

2 405nm Raman Setup, method and results

2.1 Overview

The 405nm Raman microspectroscopy setup contains many different components that will be covered in the subsections in this chapter. Figure 5 shows a schematic overview of the entire 405nm setup. All the main components are shown with component details covered in the subsections.

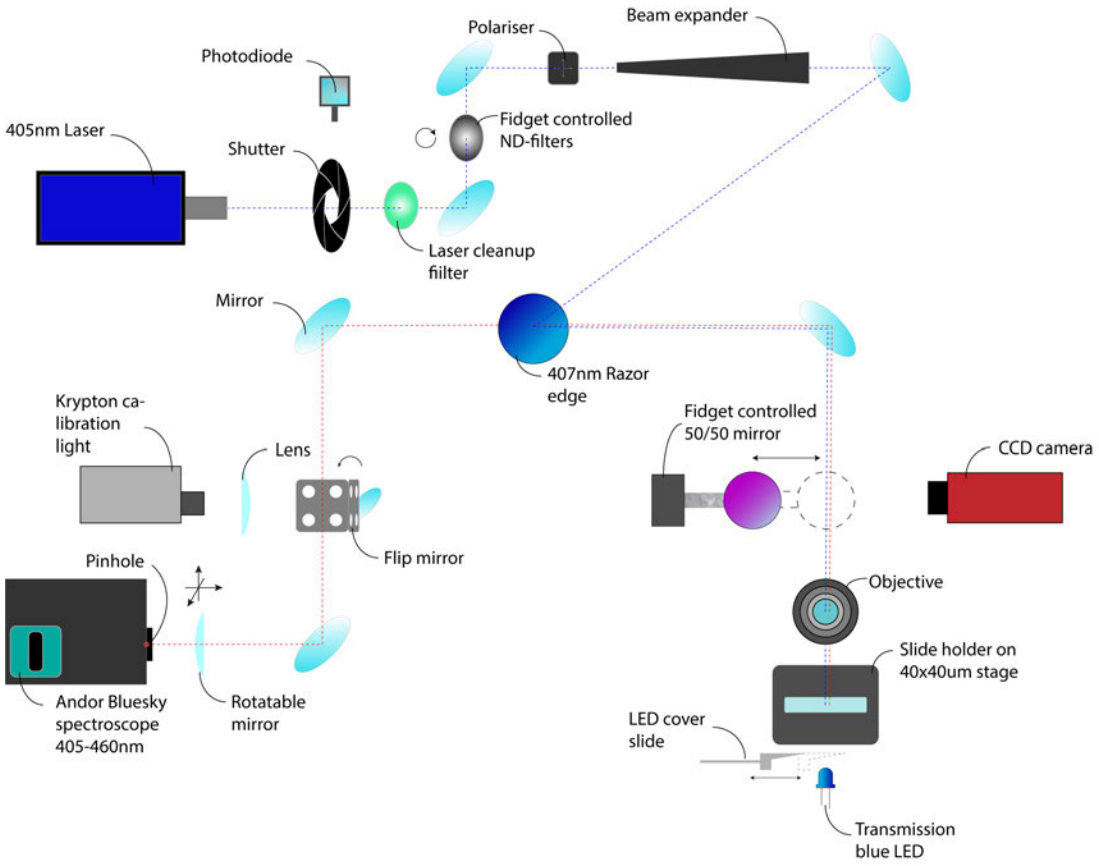

Figure 5: Schematic 405nm Raman setup. The dotted blue line represents the laser light. The dotted red line represents the Raman scattered light.

2.2 Laser

2.2.1 Method

The laser generates the 405nm laser bundle that is used to induce the Raman signal. Being an essential component many of its aspects are tested. Technical details laser: Omicron laser-diode module 405nm, CW, 40mW, high stability laser diode module, wavelength stabilised, optical bandwith <150MHz (FWHM), coherence length >60cm, beam diameter = 1.25mm ($1/e^2$) ± 0.25mm. The laser was bought in 2012.

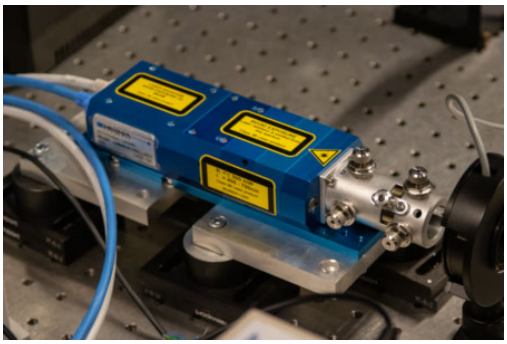

Figure 6: Omicron 405nm laser without optical fiber.

Figure 6 shows the laser in the setup. It includes an Omicron Fiber Coupling unit for FC/APC fibers. On the right side of the image the fiber coupling unit is displayed. The two knobs on both the top and left side are used to align a coupled optical fiber. The laser is computer controlled with the laser software as shown in figure 7.

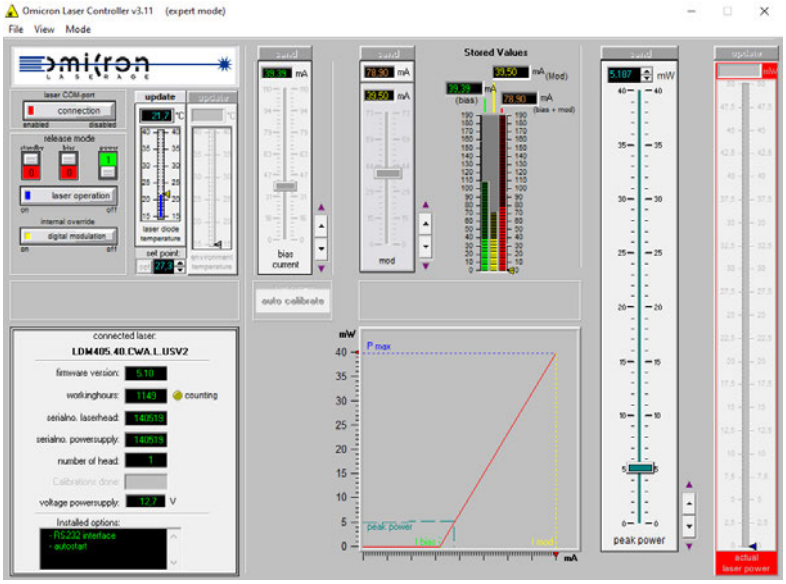

Figure 7: Omicron laser software. The green slider on the right controls the input power of the laser.

2.2.2 Results

2.2.2.1 Optical fiber stability

During early measurements using the optical fiber, it was quickly noted that the stability of the output power was fluctuating heavily. Measuring the laser output for 3 hours at 5mW input resulted in the graph shown in figure 8a. As comparison the optical fiber was removed. Results of this test are shown in figure 8b.

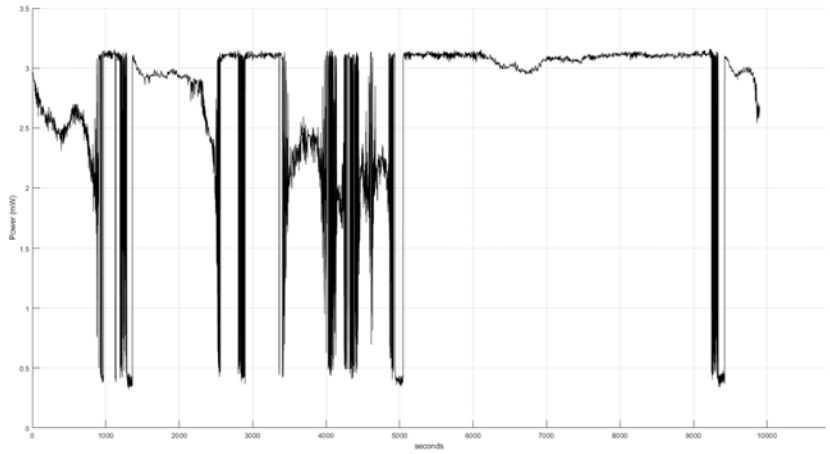

(a)

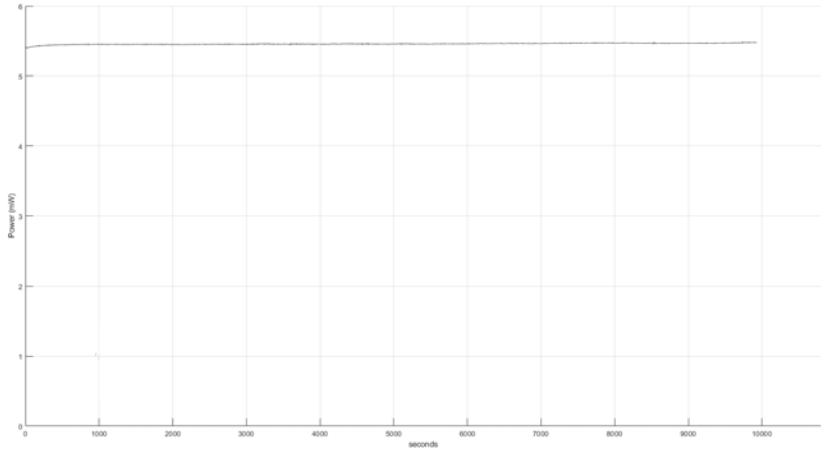

(b)

Figure 8: [10-06-2021] 5mW input singal.**(a)** 3h measurement with optical fiber encoupled.**(b)** 3h measurement without optical fiber.

Similar results appear for longer periods of time (18 hours) and at different power inputs (40mW). These graphs are shown in appendix A, figures 65 and 66.
Figure 8 shows what difference removing the optical fiber makes on the stability of the laser output. Regardless of the loss of power, the stability over a long period of

time should be near flat. A possible reason for the instability could have to do with improper alignment of the fiber. This reason is less likely as wrong alignment of the fiber significantly hampers the signal output power and is quickly noticed during setup of the laser. Other reasons include: the backscattering of light into the laser cavity or damage to the optical fiber.

2.2.2.2 Power output and input

Another issue encountered with the laser was that the power input into the software did not correlate with the output measured after the laser. Figure 8b shows that the output of the laser is around 5,5 mW whereas the input was set at 5 mW. Figures 67 and 68 in the appendix show a different behaviour where the output power is lower than the input. Between 17.9 and 18 mW where the input was 20 mW and between 32.4 and 32.5 mW when the input was 40 mW. Expressing these three measurements in percentage output vs. the input gives 110%, 90% and 82,5%. Making for non-linear behaviour in terms of the input vs. output.
Other problems with the power input vs. output arose when the power below the objective was measured for different directions. Directions being from high to low power and vice versa. Table 1 shows the difference in output when 35 mW is approached from different directions. This behaviour might come from distinct steps or modes in the laser's current supply to achieve a certain power. Maybe the laser stays in a higher mode when coming from a previous higher power input.

Table 1: Power input and output for different directions

First input (mW)	**Second input (mW)**	**Output (mW)**
40	35	12
30	35	10

2.3 Shutter & trigger

The shutter blocks or passes through the laser light. The shutter opens when measurements need to start and closes when measurements have finished. The shutter is controlled through the LabView environment. When the shutter is opened a green LED light will shine, indicating to the user that the laser is shining on the sample. The shutter is shown in figure 9a. The shutter's opening speed lies between the 8-12 ms. After this period the shutter will be fully opened, from 0 to 23 mm in diameter. To let the laser beam pass (1.25 mm diameter) it would take a maximum of $1.25 * \frac{12ms}{23mm} \approx 0.65ms$ for the light to be let trough. Technical details shutter driver: Uniblitz VMM-D1. Technical details shutter: Prontor Magnetic.
The trigger is a silicon photodiode which detects if laser light shines through the shutter. It detects reflected laser light from the laser cleanup filter. When a quick change in light intensity is detected, the photodiode will transmit a signal to the Trigger Box to trigger the 40x40 um stage to start its moving sequence. The reaction speed for the diode to detect the light and start the measurement is 1 ms. The trigger is shown in figure 9b.

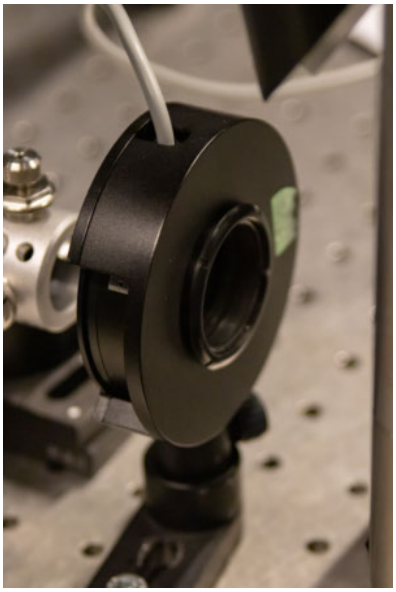

(a)

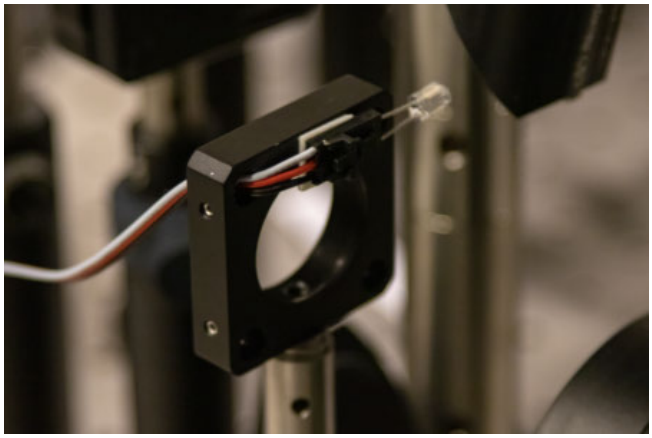

(b)

Figure 9: **(a)**Electronic shutter.**(b)** Trigger photodiode.

2.4 Laser cleanup filter

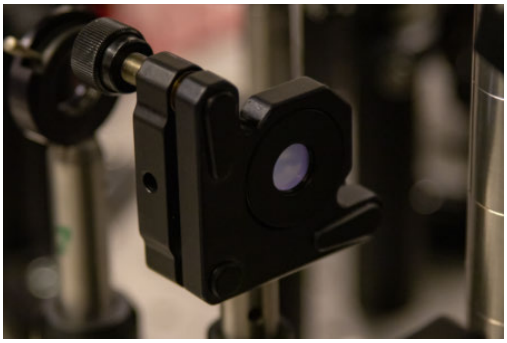

Figure 10: Laser cleanup filter.

The laser cleanup filter (bandpass) removes all unwanted wavelengths from the laser source. When generating the 405nm laser light, some additional light with a different wavelength is generated as well. This background signal can cloud measurements when trying to analyse lower wavenumbers in the Raman signal. This unwanted background can be seen in figure 11. This image is a readout from the spectroscope. The X-axis displays the pixels and the Y-axis the counts in log scale. The left peak at x=5 shows the 405 nm laser signal and the bulk signal to the right is the background that needs to be removed by the laser cleanup filter. The laser cleanup filter is shown in figure 10.
Technical details laser cleanup filter: Semrock 405nm MaxLine laser cleanup filter, part number: LL01-405, 12.5 mm X 3.5 mm. Figure 13 shows the laser cleanup characteristics at 0°.

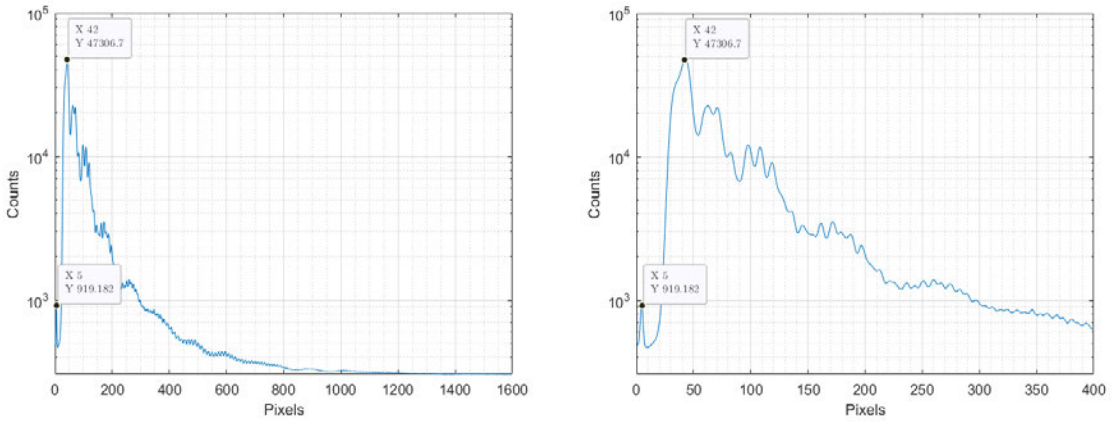

(a) (b)

Figure 11: [26-10-2022] Signal on spectroscope without laser cleanup filter.

Adding the laser cleanup filter to the setup results in the signal shown in figure 12. The experiment was performed with 6.222 mW input and 2.14 mW below the objective. The unwanted background signal has been removed. One thing to keep in mind is that the laser signal at x=5 is not actually lower in signal than the background. The laser signal is quenched by the 405 nm razor edge filter described in chapter 2.18. The background signal that is reflected by the laser cleanup filter is used for the trigger as described in section 2.3.

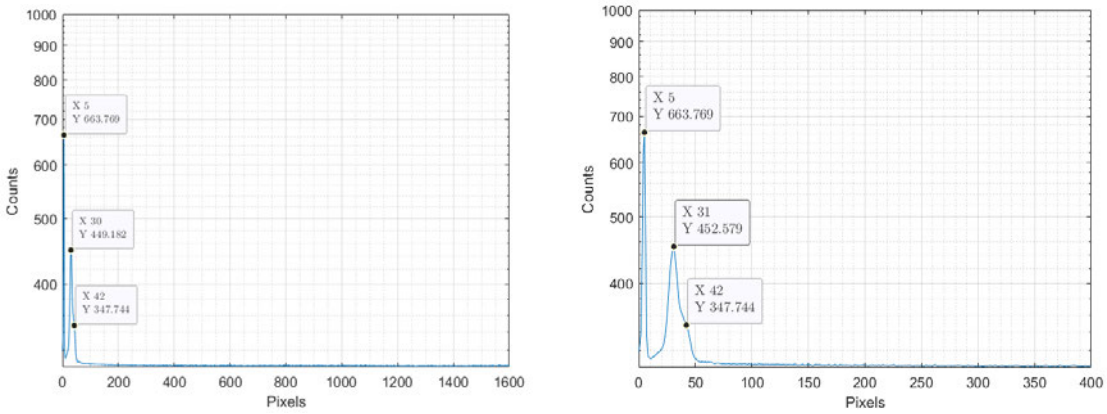

(a) (b)

Figure 12: [26-10-2022] Signal on spectroscope without laser cleanup filter.

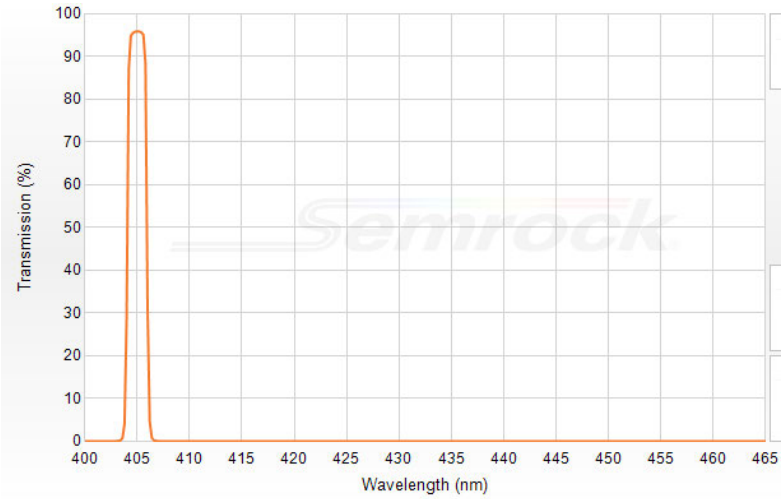

Figure 13: [12-01-2022] Semrock 405nm laser cleanup filter at 0°. Graph obtained from Semrock website.

2.5 Polariser

The polariser in this setup is placed after the ND-filters and is used to change the polarisation orientation of the laser light. The spectroscope has set directions in which it is most sensitive. Turning the polariser such that the laser light's polarisation aligns with the spectroscope's optimal polarisation will yield the highest Raman sensitivity. The polariser is shown in figure 14. Technical details polariser: WPHSM05-405 Thorlabs zero order half wave plate for 405 nm, mounted in an indexed rotation mount.

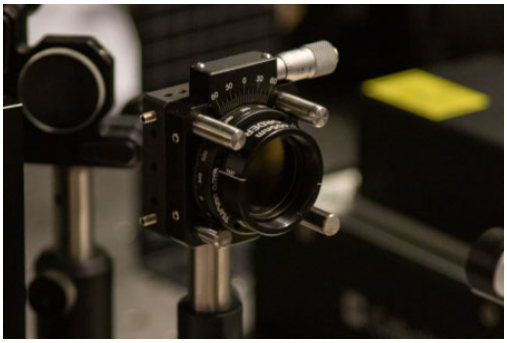

Figure 14: Polariser.

2.6 Beam expander

The beam expander is used to widen the diameter of the laser beam. This is necessary to fill the opening at the top of the objective. This creates the sharpest field of focus and ensures the light is focused in a smaller spot. The beam expander is shown in figure 15.

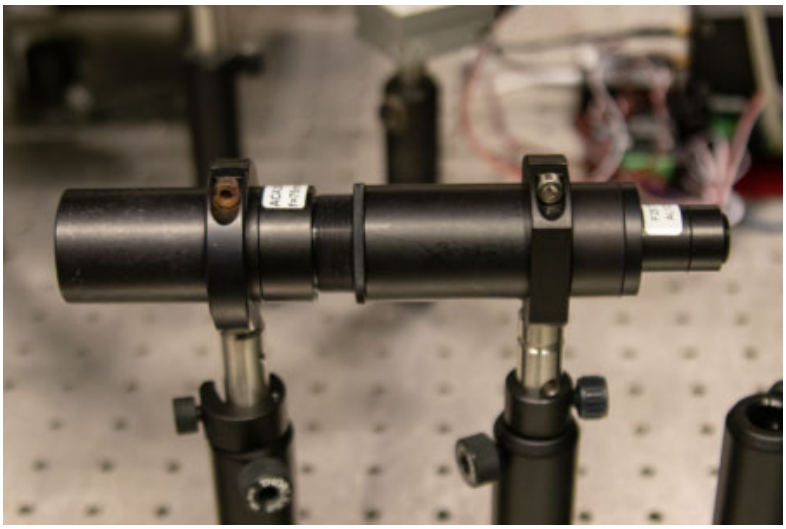

Figure 15: Beam expander.

The beam expander consists of 2 lenses separated a set distance in order to achieve a diameter closest to the objective opening. With the laser beam being 1.25mm in diameter and the opening of the objective (Olympus 40X, 0.95NA, cover slip corrected) 8,55 mm. The magnification of the laser beam should be around 7 times. The used lenses

are: f=25 and a f=75. These were set 100 mm apart. This created a magnification of 3 times, meaning the final beam diameter is 3.75 mm.
Thus, the beam expander currently lacks the right magnification for the objective used. The current magnification is 3x where ideally the spot is magnified 7 times. The reasons for this sub optimal magnification are: the available lenses at the time and the blurry spot that the laser produces. It was visually observed that the laser spot was not proper Gaussian. Unsure about the exact width of the beam after the beam expander, it was chosen to limit the magnification such that all of the available light would fit the objective opening. Ideally the beam expander is adjusted every time an objective changes.

2.7 407nm razor edge filter

The 407nm razor edge filter, shown in figure 16, is essential in the setup. It is used to reflect the 405 nm laser beam towards the objective and onto the sample. Raman light scattered from the sample must be transmitted by this razor edge filter. Only Raman signal will reach the detector if the filter is used properly. However, a portion of the 405nm light will still be transmitted. This is inevitable but also useful during calibration of the setup. A 407 nm razor edge instead of a 405 nm razor edge was chosen because the 407nm was already available in-house. The 407 nm filter enables an angled setup. Light coming from the mirror after the beam expander reflects off the razor edge and is angled towards the mirror before the objective. This angle is displayed in the top right corner of figure 5. Using the 407 nm razor edge at 0°yields the filter characteristics as shown in figure 17. With figures 17a and 17b showing the Optical Density (OD) and Transmission axis respectively. Turning the razor edge filter shifts the transmission curve towards the lower wavelengths. An angle of 14°yields the characteristics as shown in figure 18a and 18b. This setting will reflect most of the 405 nm laser light while letting through Raman scattered light that lies close to the 405 nm region. The graphs in figures 17 and 18 are taken from Semrock's light tool.

Figure 16: 407nm razor edge filter. Adjustment knobs control horizontal and vertical rotation.

This angled setup enables detection of Raman signal close to the laser wavelength as shown in figure 63b. Here the closest detected Raman shift was 142 cm^{-1}.

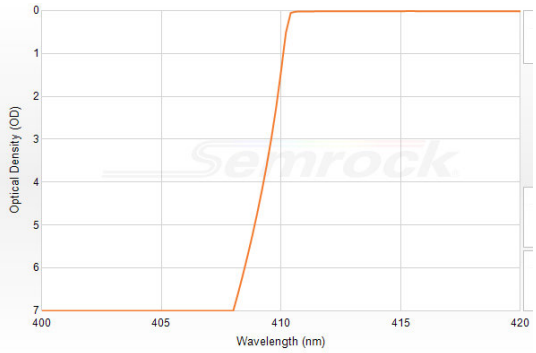

(a) Logarithmic Optical Density (OD) scale.

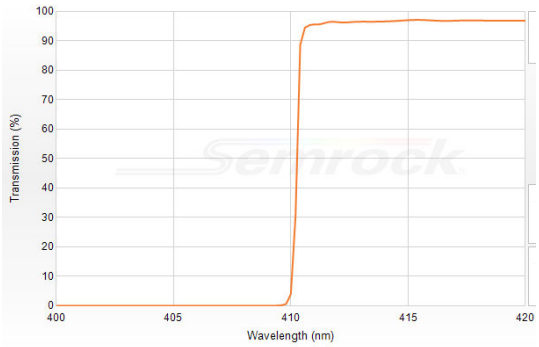

(b) Transmission % scale.

Figure 17: [13-01-2022] 407 nm Razor edge characteristics at 0°.

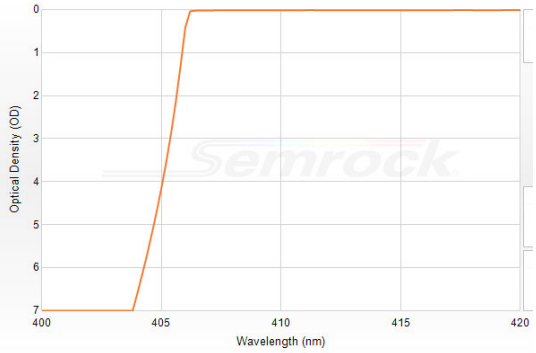

(a) Logarithmic Optical Density (OD) scale.

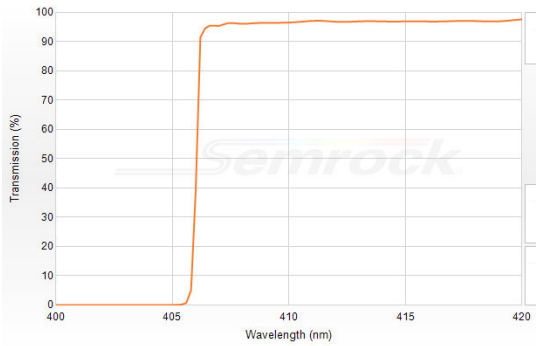

(b) Transmission % scale.

Figure 18: [13-01-2022] 407 nm Razor edge characteristics at 14°.

2.8 XYZ stage

The XYZ stage is used for course movement of the microscope slide. The X and Y direction can be controlled by the joystick shown in figure 19a. The height or Z direction is hand-controlled with a small turning wheel below the stage. This wheel is shown in figure 19b.

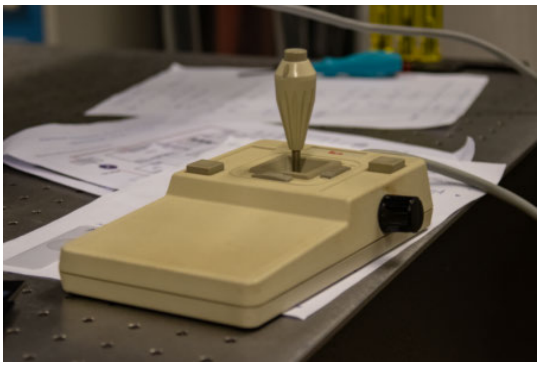

(a) Joystick to control XY-stage.

(b) Turning wheel to control stage height.

Figure 19: XYZ-stage controllers.

2.9 Objective

The objective focuses the laser light in the sample. The objective used is an Olympus 40X, 0.95NA, cover slide corrected (0.11 - 0.23mm) (UPLXAPO40X). It is shown in figure 20b. The objective's transmission is dependent on the wavelength. This dependence is shown in figure 20a.
The objective is attached to a micro controller that can be moved up or down over the range of several millimetres. The micro controller is the silver metal casing above the objective in figure 20b. The micro controller is moved through the LabView software.

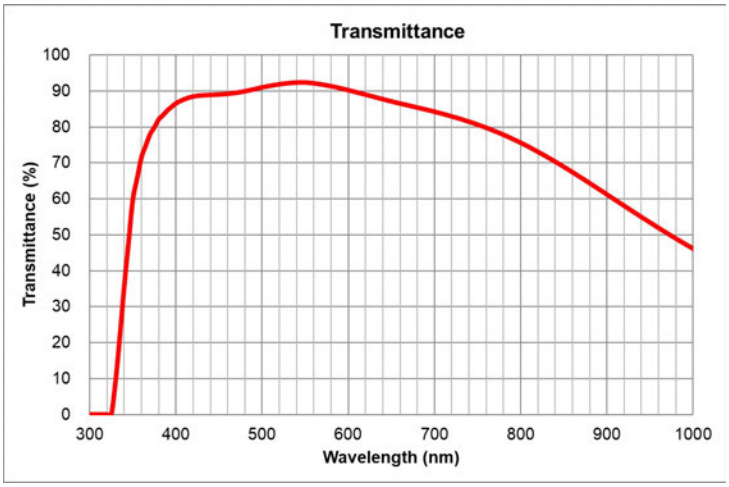

(a) [19-09-2022] Transmission curve Olympus objective UP-LXAPO40X.[11]

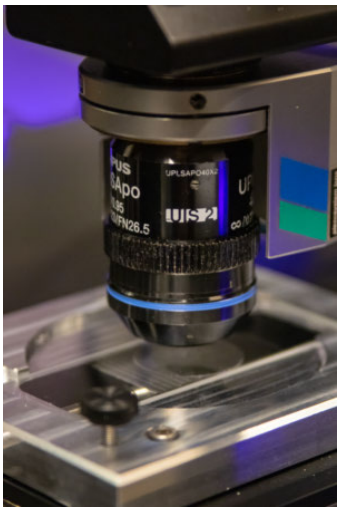

(b) Objective with silver micro controller.

Figure 20

2.10 40x40 μm stage

A 40x40um stage is used for sub-micrometer precision movement of the sample. A chosen Region Of Interest (ROI) is scanned with this stage. The stage is shown in figure 21. It holds the microscope slide holder and sits over the blue transmission light. The 40x40um stage is controlled with the LabView software. Both the box size of the ROI and the step size in X and Y can be chosen in the software. For example: choosing a 10x10 um area with 50 steps in each direction gives a 200 nm step size with a total of 2500 pixels. The stage's movement pattern starts in the top left corner. Scanning from top to bottom and then moving over to the next column in a snake like pattern. Technical details: PI P-730.4C XY nanopositioning stage.

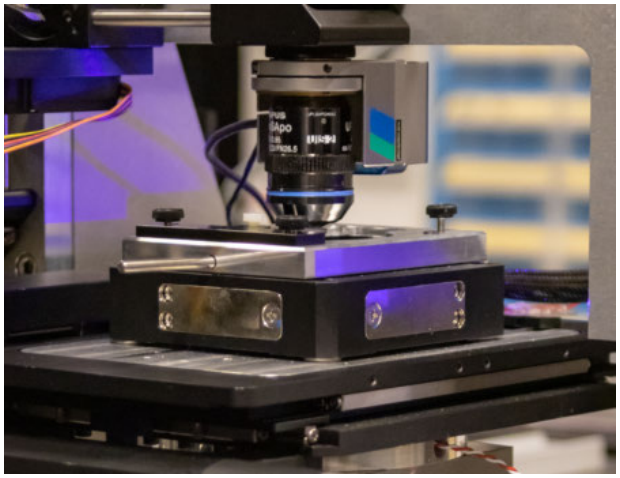

Figure 21: Black 40x40um stage below the slide holder and objective.

2.11 Blue transmission light LED

The blue transmission light is used to observe cells and other objects of interest. The transmission light sits below the slide and inside of the XYZ stage. It shines through a condenser lens onto the bottom of the microscopic slide. The condenser is needed for the focusing of the light into the objective opening. The top of the condenser lens in the setup is shown in figure 22.

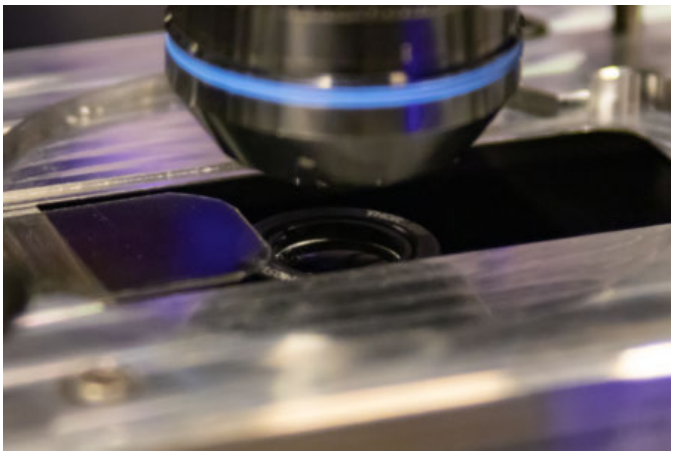

Figure 22: Top of the condenser lens below the objective and the slide holder.

2.11.1 Blue light cover slide

The condenser lens also poses a problem. When laser light shines through the condenser onto the LED, it will induce Raman scattering from the LED material. Giving a background signal as shown in figure 23a. A cover slide has been designed, that can slide over the condenser during measurements, to prevent the extra signal from occurring. The cover slide is attached through the microscope slide holder and can be controlled manually. The manufactured model in the setup is shown in figures 24a and 24b. When the slide covers the condenser, the signal on the spectroscope goes back to flat as shown in figure 23b.

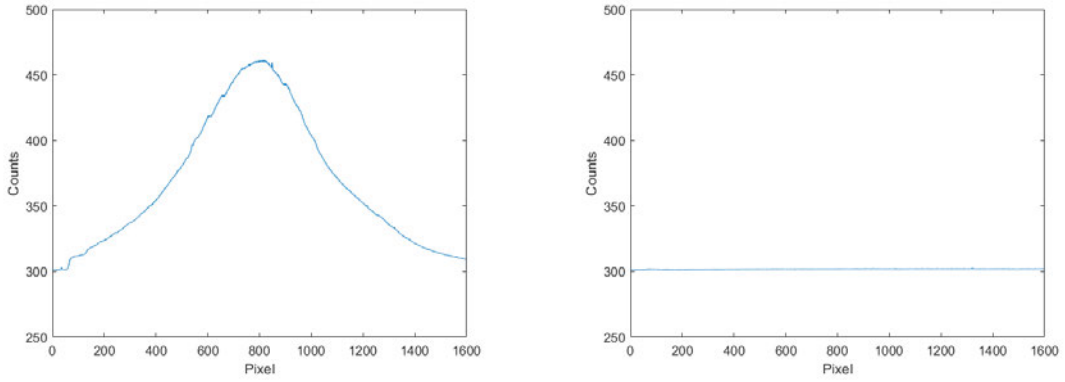

(a) (b)

Figure 23: [21-07-2021] **(a)** Spectrum without cover slide on empty microscope glass.**(b)** Spectrum with cover slide pushed over condenser.

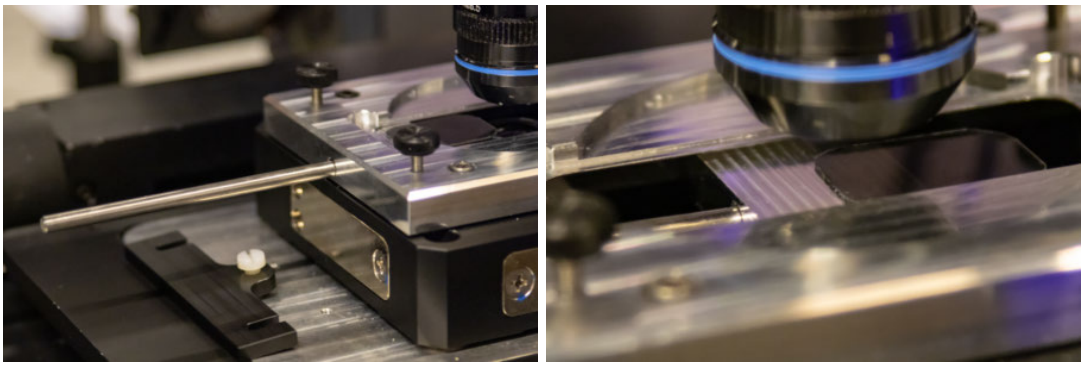

(a) (b)

Figure 24: **(a)** Cover slide operating rod.**(b)** Cover slide covering the condenser.

2.12 Slide holder

The slide holder is used together with a few other components: it sits on top of the 40x40um stage, covers the blue LED, holds the cover slide and holds the microscopic slides. The manufactured version in the setup is shown in figure 21 above the 40x40 um stage. Another addition to the slide holder were the slide clamps. These clamps prevent the microscope slide from moving during experiments. A clamp is shown in figure 25. The slide holder accommodates standard size microscope slides (25 x 75 mm).

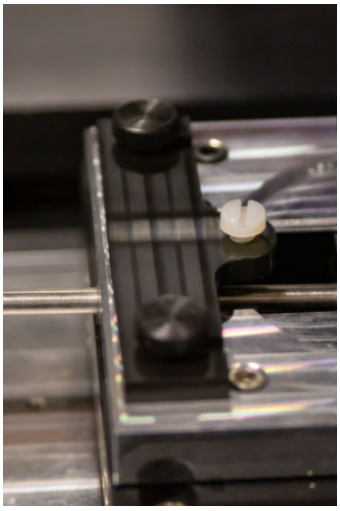

Figure 25: Microscope slide clamp.

2.13 Polarisation filters

To observe and identify birefringent objects on the microscope slide, polarisation filters are added to the setup. The first polarisation filter is fixed to the end of slide holder mentioned in section 2.12. This filter is shown in figure 26. The second polarisation filter is mounted before the CCD camera mentioned in section 2.14. This second filter is rotatable, enabling the detection of the birefringent objects. Figures 27a and 27b show the difference between a brightfield image and a polarised image. Technical details polarisation filters: LPVISE2X2 dichroic film polariser sheet and LPVISE100-A ⌀1" linear polariser.

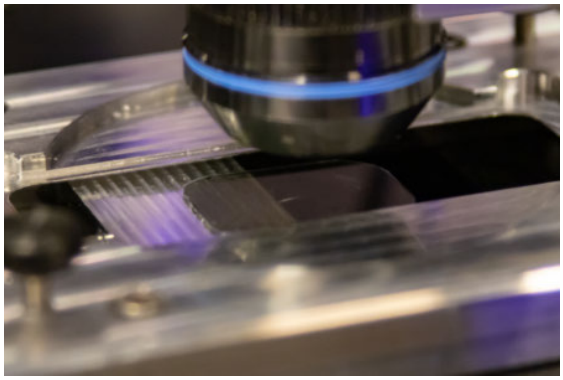

Figure 26: Polarisation sheet above condenser lens.

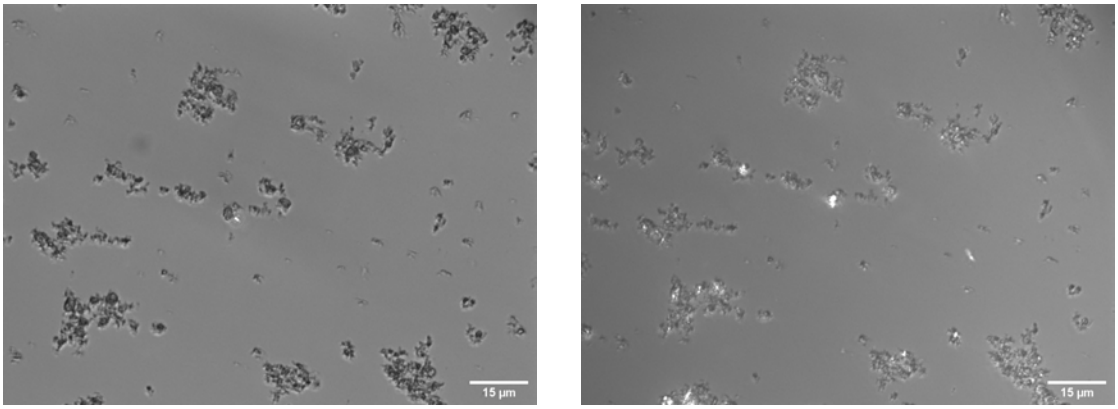

(a) (b)

Figure 27: [M1a_S1 31-01-2021] **(a)** Non polarised brightfield image. **(b)** Polarised image with birefringent objects transmitting light.

2.14 CCD camera

The CCD camera (Stingray F-125B) is used together with the transmission LED to observe the samples and determine a ROI to be scanned. Figure 28b shows the red CCD camera with the front black ring being the polariser mentioned in section 2.13. The CCD camera is controlled by the Vimba Viewer software. The CCD camera has a 1292 by 964 pixel chip. With a pixel size of 3.75 x 3.75 μm. A f-125 mm lens is mounted before the CCD chip. The 40X Olympus objective is usually combined with a f-180 mm lens before a camera to obtain the 40X magnification. In this setup a f-125 mm lens is used. This yields a theoretical magnification of $\frac{125}{180} * 40 \approx 27.78X$
Figure 28a shows a calibration image that can be used to determine the magnification and the distance per camera pixel. The three vertical bars and the three horizontal bars at number six are 17.54 μm apart. The white arrows in figure 28a represent this distance.
Taking an average of 6 measurements (3 vertical, 3 horizontal) at three locations along the black bars gives 131 pixels average distance. The measurements were taken using ImageJ. Multiplying this 131 pixels times the average pixel size of 3.75 μm gives: $131 * 3.75 = 491.25\mu m$. Dividing this distance by the actual distance of 17.54 μm gives the measured magnification. $\frac{491.25}{17.54} \approx 28.01X$.

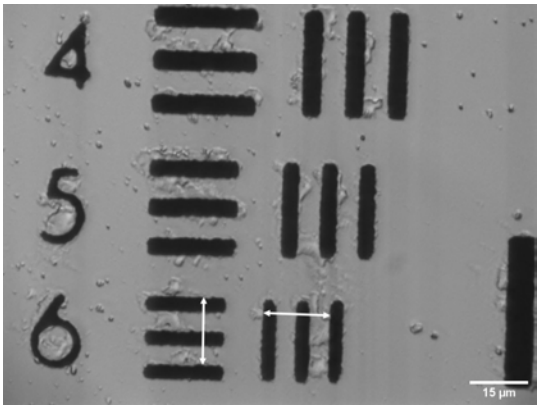

(a)

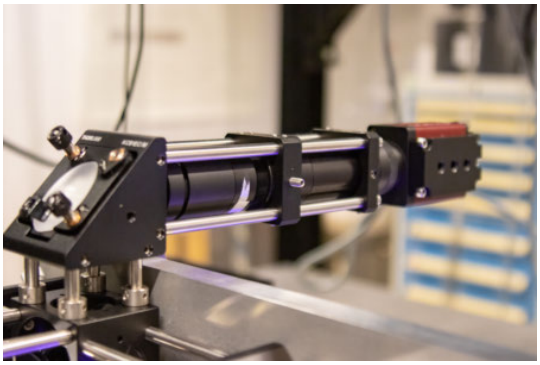

(b)

Figure 28: [24-11-2021] **(a)** Calibration image. **(b)** CCD camera for live view of sample.

While the CCD camera has a 1292x964 pixel chip, the Vimba Viewer software crops the view to a 1024x768 pixel image. This setting can be changed temporarily in the software but will jump back to the standard 1024x768 setting after a day of use. Figure 29 shows the difference between the 1292x964 and the 1024x768 pixel view. When a smaller size (less pixels) is chosen in the software, the view of the camera will be cropped from the bottom right. This is without any horizontal image flipping that is necessary to align this CCD image with the spectroscope view. When the image is horizontally flipped in the software the cropping will occur from the bottom left corner.

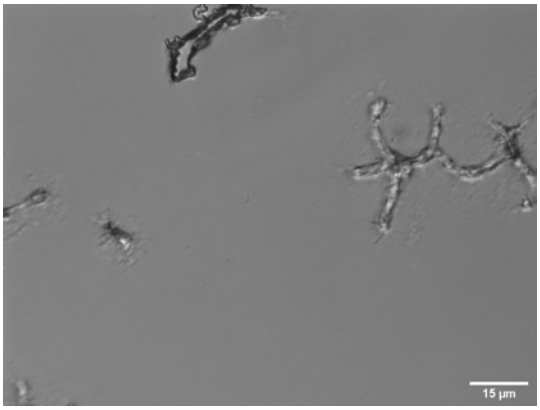

(a)

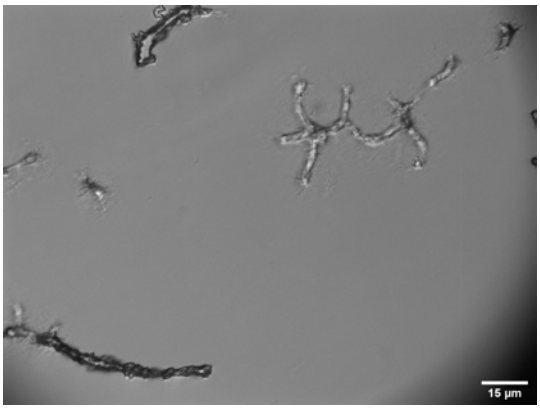

(b)

Figure 29: [20-09-2022] **(a)** 1024x768 pixel view CCD. **(b)** 1292x964 pixel view CCD.

2.15 Fidgets

The linear fidgets are used to control the position of both the different ND filters and the 50/50 beamsplitter. They are controlled through the Trigger Box and the LabView software. The following model numbers are used: Actuonix L16-50-63-12P and L16-100-63-12P.

2.15.1 ND filters

To control the laser power during measurements different ND filters are used. The ND filters are placed after the laser cleanup filter and are controlled with the fidget. It is designed to have 4 different slots for ND filters. The manufactured design with the fidget and ND filters is shown in figure 30. From top to bottom the following ND filters are used: empty, ND1, ND2 and ND3. Each step up in ND number will let through less light. ND1 $\approx$ 10%, ND2 $\approx$ 1% and ND3 $\approx$ 0.1% transmission.

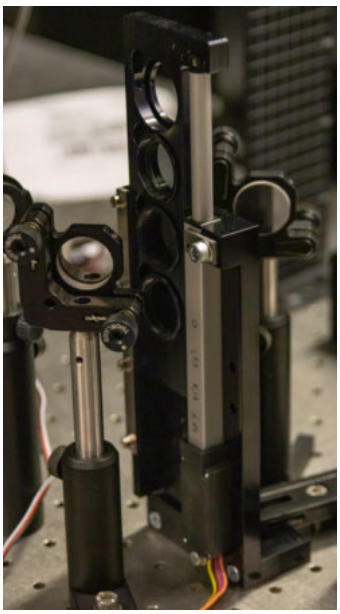

Figure 30: ND filter holder with fidget in setup.

2.15.2 50/50 beamsplitter

The 50/50 beamsplitter is used to project transmission light from the sample to the CCD camera. It will also transmit laser light to determine the measurement position. The 50/50 is controlled with another fidget and the manufactured version in the setup is shown in figure 31. Technical details 50/50 beamsplitter: Thorlabs ⌀1" pellicle.

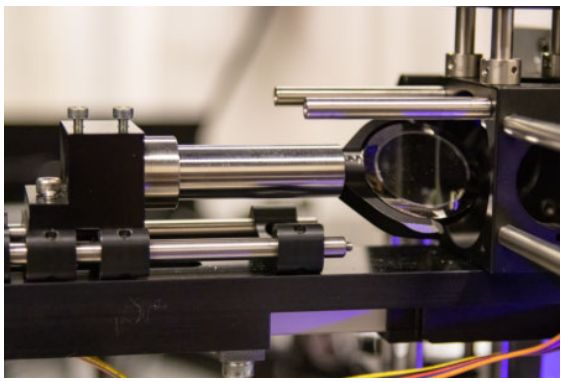

Figure 31: 50/50 beamsplitter with fidget in setup.

2.16 Blue LED calibration light

Another blue LED is used during the calibration of the setup. Controlled through the LabView software, this LED's characteristic spectral curve is used for data processing in the QCR program. The LED's spectral curve is shown in figure 32a. The LED is mounted onto a microscope slide for calibration below the objective. The design is shown in figure 32b. Technical details LED: ILH-XC01-S410-SC211-WIR200. Intelligent LED Solutions, C3535 1 Powerstar Series UV LED, 420nm 440mW 125°, 4-Pin.

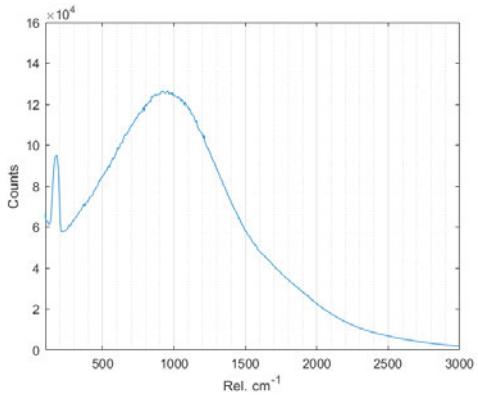

(a)

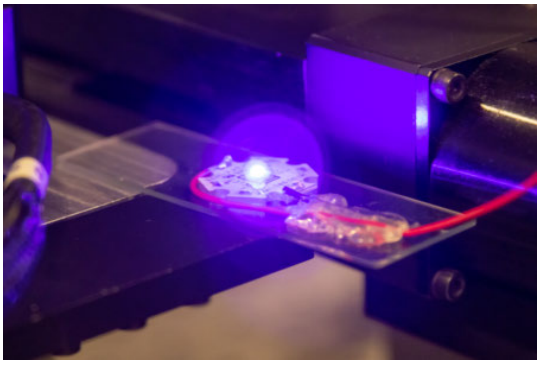

(b)

Figure 32: [31-01-2022] **(a)** Calibration LED spectrum.**(b)** Calibration LED in setup.

2.17 Krypton lamp

The other light source used for the calibration is the krypton lamp. This krypton lamp can be measured with the spectroscope by flipping a mirror into the detection path. A lens sitting in between the krypton lamp and the flip mirror focuses the krypton light into a parallel beam. The krypton lamp gives off a specific spectrum which is shown in figure 33a. The krypton lamp and the flip mirror used are shown in figures 33b and 33c respectively. The Krypton lamp used is an Ocean Optics KR-1 calibration light (427-893nm).

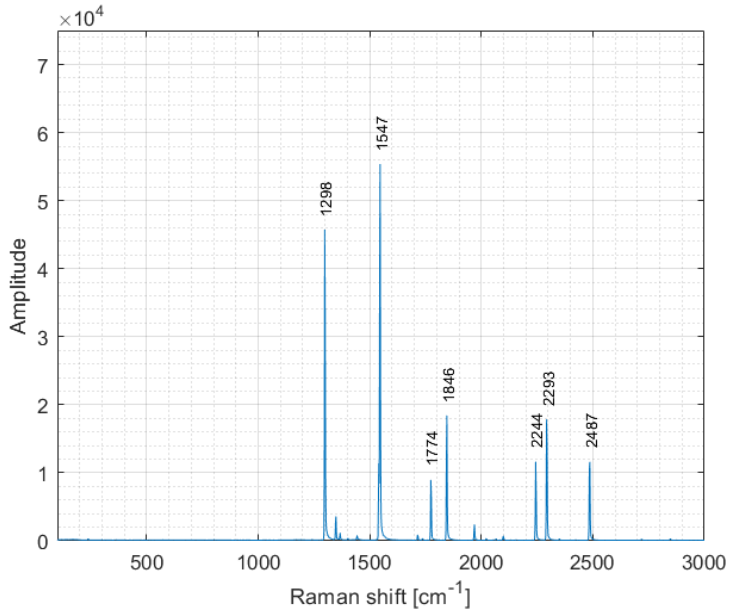

(a)

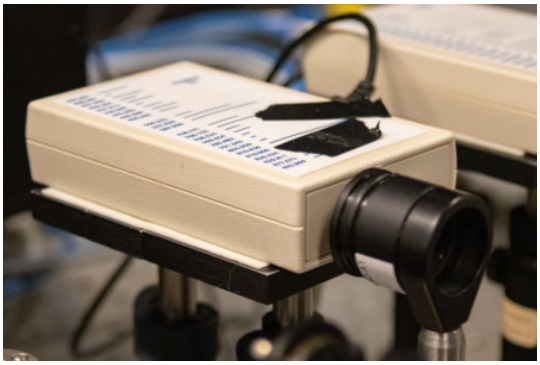

(b)

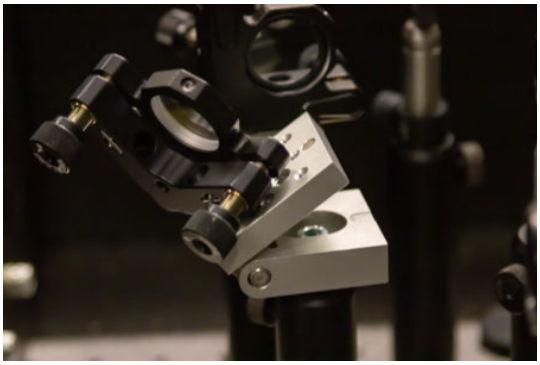

(c)

Figure 33: [31-01-2022] **(a)** Krypton light spectrum.**(b)** Krypton light with focus lens in setup.**(c)** Flip mirror.

2.18 405 nm long pass razor edge

The 407nm razor edge filters out a large portion of the laser light when reflected off the microscope slide. Some light will still be transmitted through the 407nm razor edge and detected by the spectroscope. To reduce the signal from the laser even further, an additional long pass razor edge filter is added. The filter characteristics are given in figure 35. The graph in figure 35 is taken from Semrock's light tool. Technical details filter: Semrock 405 nm RazorEdge ultrasteep long pass edge filter. The signal on the spectroscope without the filter is shown in figure 36a. With the filter added the signal looks as shown in figure 36b. Both measurements were conducted with 5 mW input power and 1.69 mW below the objective. The signals have been averaged over 144 measurements with 38.78 ms exposure time per measurement. Figure 34 shows the long pass razor edge in the setup.

Figure 34: 405 nm long pass razor edge filter.

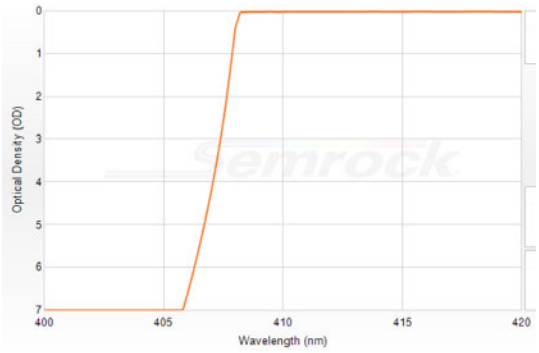

(a) Logarithmic Optical Density (OD) scale.

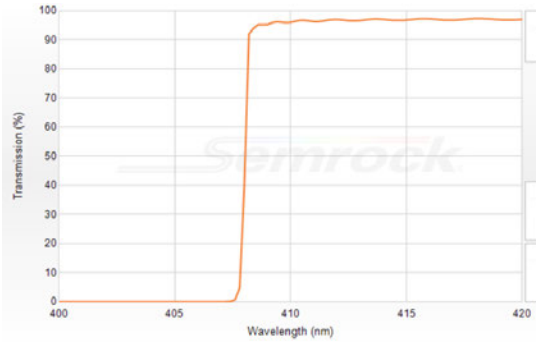

(b) Transmission % scale.

Figure 35: [27-09-2022] 405 nm RazorEdge characteristics at 0°.

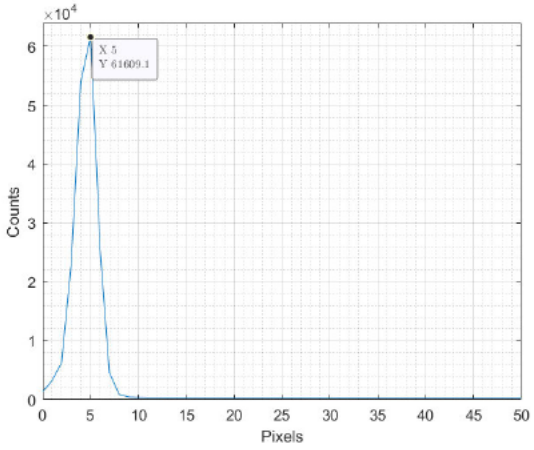

(a) Without 405 filter.

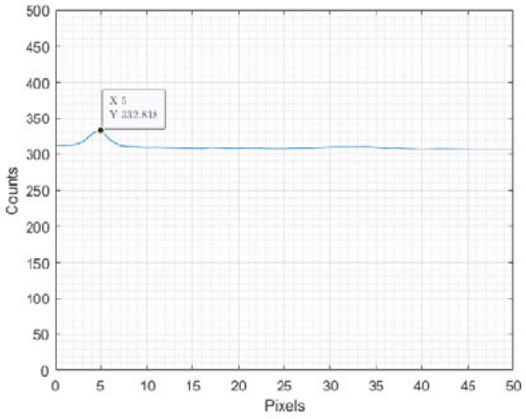

(b) With 405 filter.

Figure 36: [13-10-2022] 405 nm RazorEdge influence in setup.

2.19 Prism box

The prism box is used to separate the different wavelengths of Raman light that enter the pinhole. Inside are three prisms that separate the wavelengths and direct the light onto the spectroscope's CCD slit. The pinhole used is 15um in diameter. The design of the prism box is shown in figure 37. A ND filter behind the pinhole is used to decrease the power of incoming light. This ND filter can be turned in front of the pinhole with a switch on the outside of the box. It is used during alignment of the setup to prevent too much light exposure on the spectroscope. Technical details ND filter: Thorlabs ND3/OD3 NE30A.

[redacted] 37: Inside of the prism box with the light path in blue. Golden switch circled in red controls the ND filter.

2.20 Pinhole focus lens

The pinhole focus lens controls the focus of the incoming light on the pinhole. Both its horizontal and vertical rotation are controlled with adjusters. These adjusters are manually controlled and have both course and fine movement options. The pinhole focus lens is shown in figure 38. It is a Thorlabs 100mm focal length with a 25mm diameter lens.

Figure 38: Pinhole focus lens.

2.21 Spectroscope

The spectroscope is used to detect and count each Raman scattered wavelength. The spectroscope is air-cooled and operates at -80°C. It is mounted on top of the prism box. Spectroscope control is integrated within the LabView software. The spectroscope model is an Andor Newton CCD 970N and is shown in figure 39. The spectroscope has 1600 pixels and the spectroscope's detection range is measured going from 404.83 nm to 461.42 nm. The rel. cm^{-1} is measured going from -4.7079 rel.cm^{-1} until 3024.6 rel.cm^{-1}. This sets the average resolution of the spectroscope at 0.0354 nm/pixel and 1.8933 rel.cm^{-1}/pixel. Figure 40 shows the measured data for both the wavelength and rel.cm^{-1} vs. the pixels.
The Quantum Efficiency (QE) of the setup can be calculated from the calibration files as well. This is then used to scale measurement files and account for any differences in detection sensitivity. Figure 41 shows the QE against the wavelength and the Raman shift.

Figure 39: Andor spectroscope.

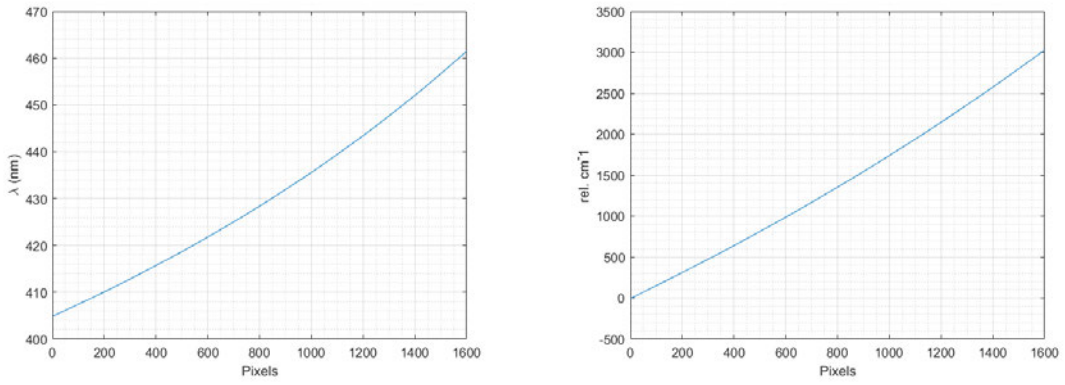

(a) (b)

Figure 40: [28-09-2022] **(a)** Wavelength vs. pixel.**(b)** Rel.cm^{-1} vs. pixel.

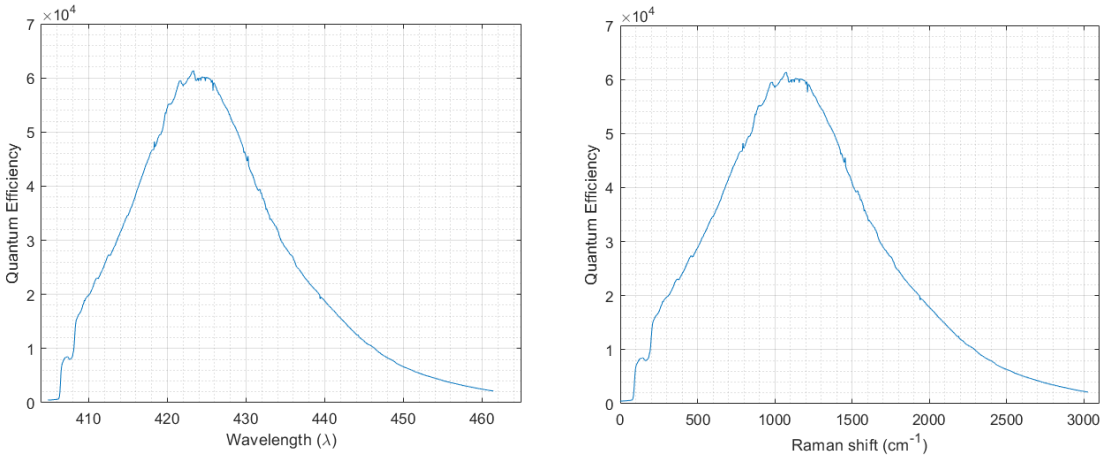

(a) (b)

Figure 41: [13-10-2022] **(a)** Wavelength vs. QE.**(b)** Rel.cm^{-1} vs. QE.

3 Method calibration and cells

3.1 Toluene measurements

Toluene measurements were performed using a microscope well slide. The well in the middle of the slide is covered halfway with a cover glass. 20 μL of 99.5% pure Toluene is pipetted in between the slide and the cover glass and into the well. After the toluene is pipetted the cover glass is pushed over the rest of the well. This prevents air bubbles sitting in the well and influencing measurements. The microscopic slide with the toluene filled cavity is then placed onto the slide holder. Regular Toluene calibration measurements are performed at 10 mW laser power below the objective. Spectroscope exposure time is set at 250 ms and 144 (or 12x12) measurements are taken.

3.2 Red Blood Cells

Red Blood Cells in earlier phases of the project are obtained through a finger prick on a voluntary donor. 250μL is collected and 50 μL is added to 500 μL of 1X PBS. The solution is vortexed for a few seconds before being centrifuged for 10min @800 g. All fluid above the pallet is aspirated and 150 μL of 1X PBS is added. 100 μL of 4% PFA (paraformaldehyde) is added to fixate the cells. Then a waiting step of 15min at room temperature. 500 μL of PBS is added and the solution is vortexed for a few seconds and centrifuged for 10 min @800 g. Afterwards the solution above the pallet is aspirated and 1X PBS is added to a desired concentration (most often 300 μL is used).

3.3 White Blood Cells donor

A WBC solution (1.5 mL)in PBS was obtained from a fellow researcher containing 10x10^6 $cells/mL$. The solution is centrifuged for 5 min @300 g. Everthing above the pallet is aspirated. 100 μL of 4% Formaldehyde (FA) is added to the pallet and a waiting step of 10min at room temperature is performed. 5 mL of PBS is added to dilute. The solution is centrifuged again for 5min @300 g. All solution above the pallet is aspirated. 1 mL of PBS is added and the solution is transferred to a small eppendorf tube giving a final concentration of 15x10$^6 cells/mL$.

3.4 QCR program analysis

Analysis of the spectral data obtained by the spectroscope is done through the in-house developed QCR (Quantitative Calibration Routine) program. All calibration and measurement files are imported into the program after which the spectral analysis is performed. Two main windows in the QCR program are shown in figures 42a and 42b. In figure 42a the user selects a region of interest with the yellow crosshair. The red crosshair is placed on a background region of the image, or a region one wants to compare to the yellow crosshair. The spectra of the red and yellow crosshair are shown in figure 42b. The green spectrum is the result of the yellow spectrum minus the red spectrum. Also shown in figure 42b are two vertical blue bars enclosing the highest peak. These blue bars can be manually shifted across the spectrum. The area in between the blue bars (the width can be altered) is shown in figure 42a as the visual colours. Areas that contain a Raman peak within the blue bars will show up more red in the left image. This can be used to identify specific enzymes within different locations in a cell. At the top of figure 42a an input for the 'Box Size @Crosshair' can be set. This input is the pixel width and height of a box surrounding the crosshair upon which the signal is averaged.

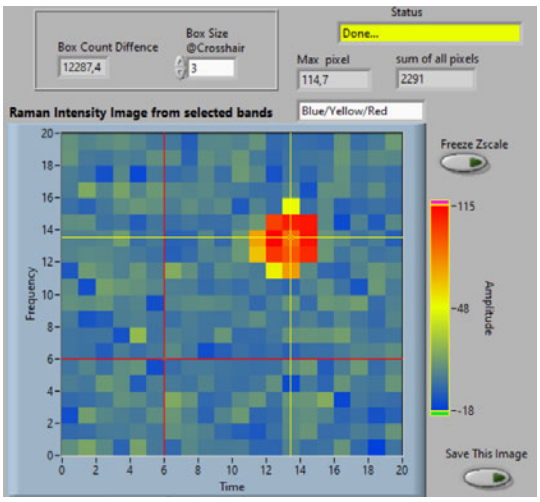

(a) Crosshair selection box

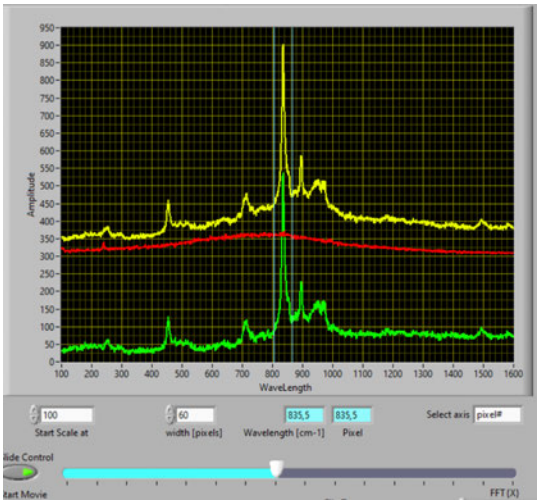

(b) Spectrum from crosshair positions

Figure 42: Two main windows inside the QCR program.

3.5 Principle Component Analysis (PCA)

In order to visualise different components inside a cell an in-house Matlab script is used to perform Principle Component Analysis. This script loads data files from the QCR program and analyses them to find different regions based on the difference in the spectrum. Rather than moving the crosshairs in the QCR program to obtain a certain spectrum for that region, the PCA program does this for you. The input it requires is the number of clusters one would like to divide the image in. The following Matlab scripts were used: LoadData, PreTreatData, MultiVariate and NocPlotter. Created by Cees Otto and available within the MCBP department.

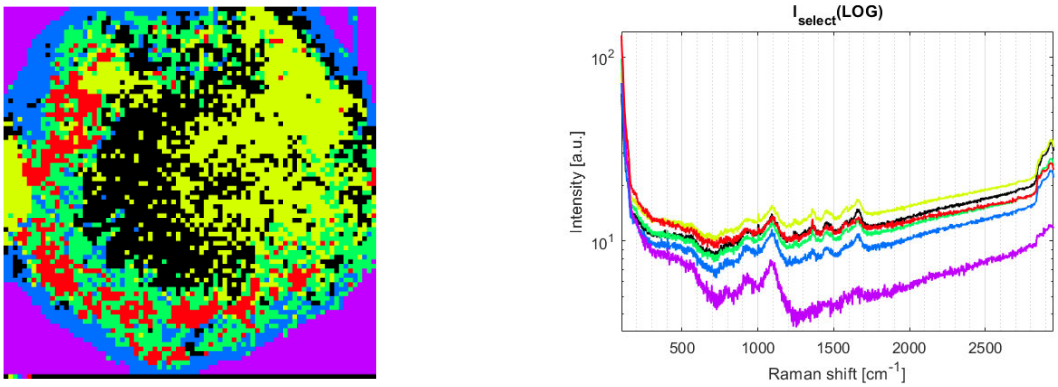

(a) (b)

Figure 43: PCA program commonly used graphs.**(a)** PCA cell divided in 6 clusters.**(b)** PCA logarithmic spectrum with different colour clusters.

4 Results calibration and cells

After the validation of every individual component the setup needed to be tested as a whole. Toluene was used at first for its distinctive Raman spectrum. Next steps in Raman signal testing were performed with RBC's. Different powers and exposure times were tested to evaluate the signal vs. the destruction/bleaching of the cell. After tests with RBC's, WBC's from both cultures and blood samples were tested.

4.1 Toluene

The Toluene spectrum measured with the 405nm setup is shown in figure 44a. This result can be compared to the spectrum from the older 647nm setup, which is shown in figure 44b. The 405nm spectrum is measured as described in section 3.1. The 647nm spectrum is measured with 35 mW below the objective, an exposure time of 250 ms and 1600 measurements were taken.

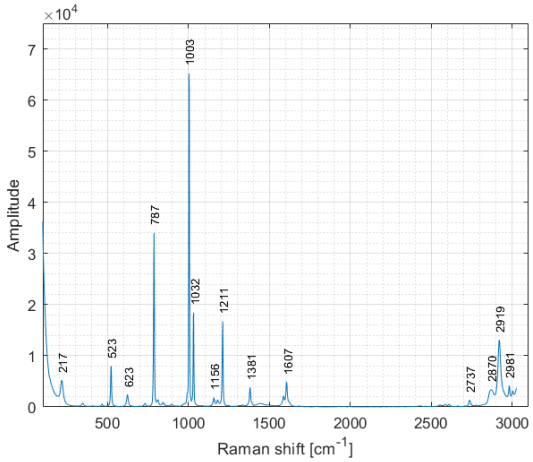

(a) [31-01-2022, tol-405-new.txt] 405 nm Toluene spectrum. 10 mW.

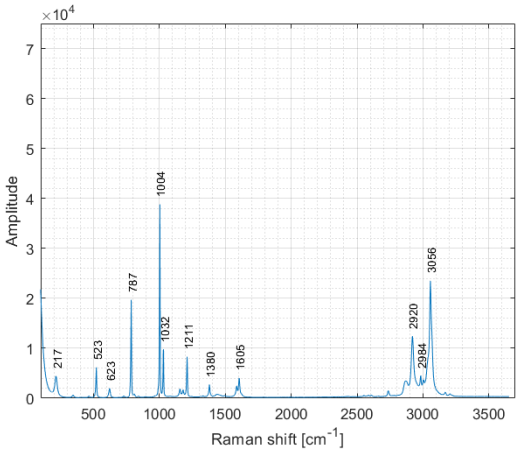

(b) [05-04-2022] 647 nm Toluene spectrum. 35 mW.

Figure 44: Toluene spectra comparison with main peak indications.

The toluene measurement comparison of the 405 nm and the 647 nm setup in figure 44 shows that the 405 nm setup is more than capable of detecting Raman signal. The 647 nm has a wider detection range than the 405nm which is why the last 3056cm^{-1} peak does not show up with the 405 nm. The measurement power of the 405 nm (10 mW) is 3.5 times lower than the 647 nm (35 mW), the exposure time is the same in both setups (250 ms) and the number of measurements around 11 times lower for the 405 nm (144) vs. the 647 nm (1600). The maximum peak height at $\sim$ 1003 cm^{-1} is around 6500 amplitude for the 405 nm and around 4000 amplitude for the 647 nm. While the 405 nm shows a higher signal detected at a lower input power, the difference in laser wavelength can cause resonant Raman to account for this signal difference.

4.2 Red Blood Cells

4.2.1 First RBC

First tests with RBC's were performed at an arbitrary choice of 1,26mW, 200 ms exposure time, 20x20 pixels at 40x40 μm scanning ROI (region of interest). Giving a resolution of $2\mu m/pixel$. The brightfield image of one RBC imaged first is shown in figure 45a. The white spot in the middle of cell shows the laser focus. Figure 45b shows the crosshair image of the largest peak at 835 pixels as shown in figure 45c. In this figure the main peaks are indicated with their respective pixel locations. Note that this is not the regular cm^{-1} format as no calibration was done for this first measurement.

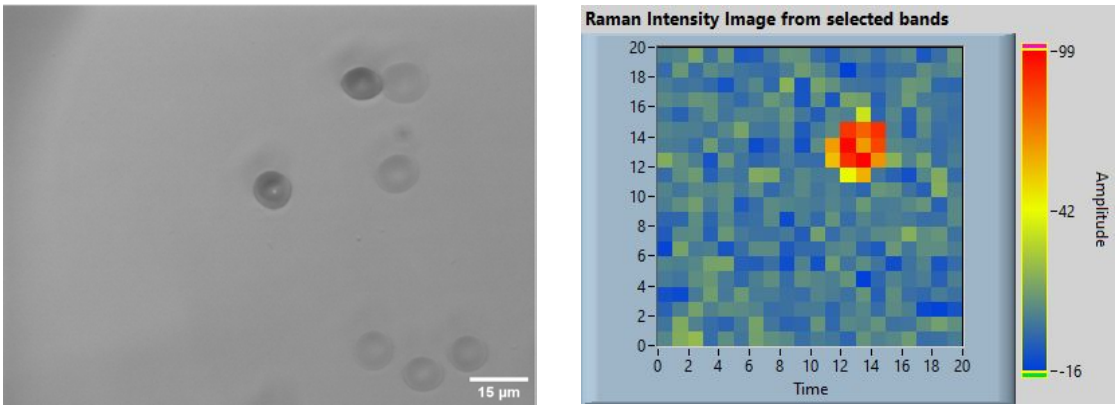

(a) (b)

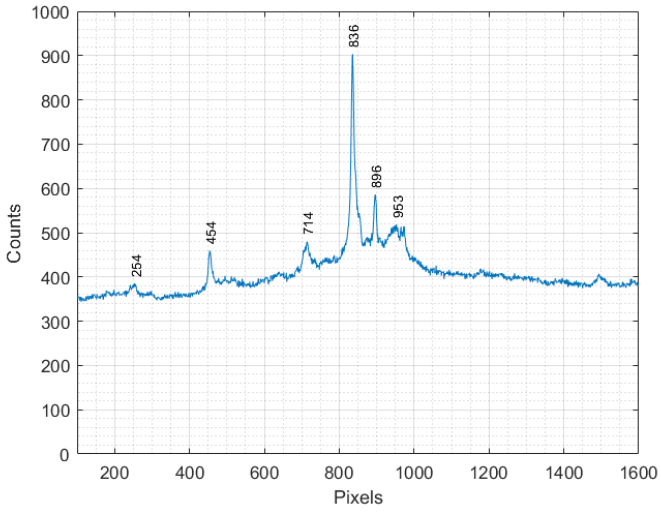

(c)

Figure 45: [23-07-2021] 1,26mW laser power, 200ms exposure time, 20x20 pixels at 40x40μm ROI. **(a)** Brightfield image first RBC.**(b)** Crosshair image of first RBC.**(c)** Spectrum first RBC.

4.2.2 Laser inflicted cell damage

While a signal can be obtained from the RBCs, the cell's appearance changes. This can be seen in figure 46. Figure 46a shows a brightfield image of a RBC and figure 46b shows the same RBC after a 500 μW measurement. The dark RBC changes to a more transparent state after the measurement is done. Due to this destruction of the cell a lower power and exposure time were tested (tests not included in this report). The power value optimal for a better signal to noise ratio was set at $195\mu W$. The exposure time mostly used is around $100ms$ but can still vary for some experiments.

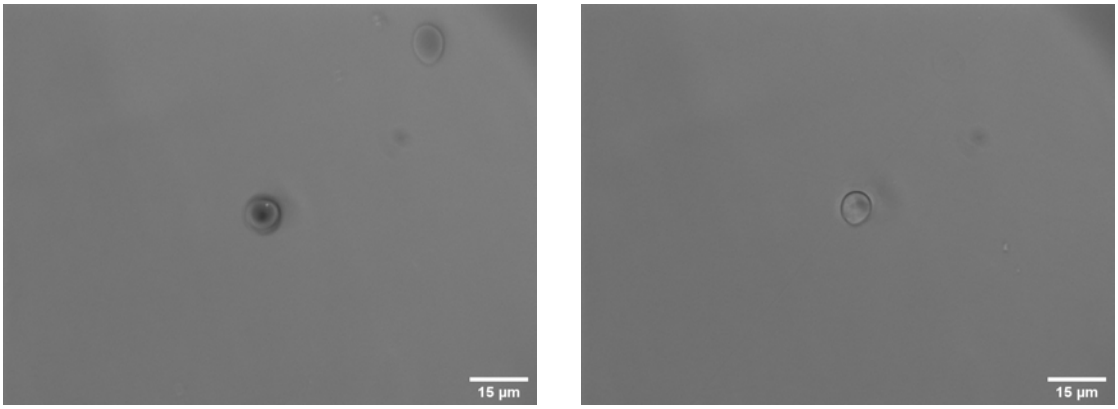

(a) (b)

Figure 46: [27-07-2021] $500\mu W$ laser power, $200ms$ exposure time, 40x40 points at 10x10μm ROI.**(a)** Brightfield image of cell before measurement.**(b)** Brightfield image of cell after measurement.

The results in figure 45 shows the potential to measure RBCs with the 405nm setup. With these relative higher input powers comes the disadvantage of cell destruction.

4.2.3 Signal regression

To investigate this destructive effect, an analysis into possible signal regression was performed. Two adjacent RBCs were scanned five times at $195muW$, $40ms$ exposure time, 80x80 steps at 16x16μm.
Figure 47 shows the brightfield images before and after the 5 measurements. The two cells in the middle of the image enclosed by the red square have been imaged. Figure 48 shows the locations of the crosshairs used for analysis. A 4 pixel box average (16 pixels) was taken. The spectral result of the five measurements is shown in figure 49. The Raman shift of the main peaks of measurement 1 are indicated above the peaks.
The regression experiment shown in figures 47 and 49 shows that with a lower input power and a lower exposure time the RBCs will still be damaged, but at a much slower rate compared to the signal loss in figure 46.

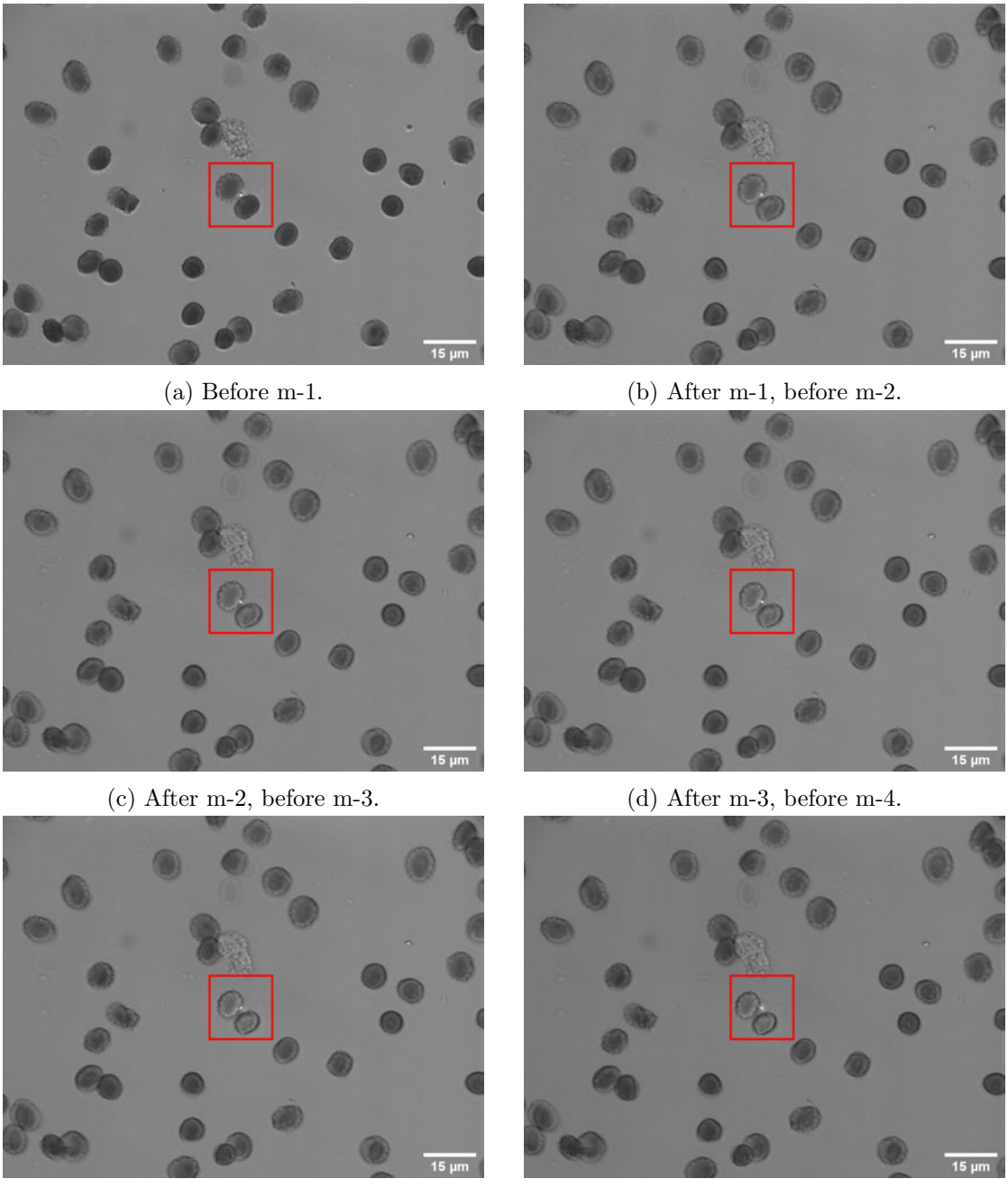

(a) Before m-1.

(b) After m-1, before m-2.

(c) After m-2, before m-3.

(d) After m-3, before m-4.

(e) After m-4, before m-5.

(f) After m-5.

Figure 47: [20-10-2021] $195\mu W$, $40ms$ exposure time, 80x80 steps at 16x16 μm ROI. Brightfield images of bleaching cell. Measurements indicated as m-x (x being the measurement number). Red squares indicate the scanned region.

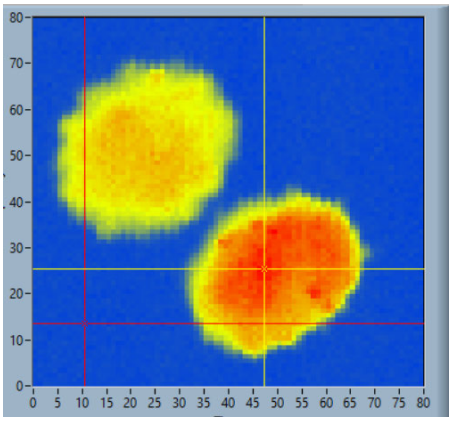

Figure 48: [20-10-2021, M1a] Crosshair location in QCR program for 5 RBC measurements. Average of 16 surrounding pixels.

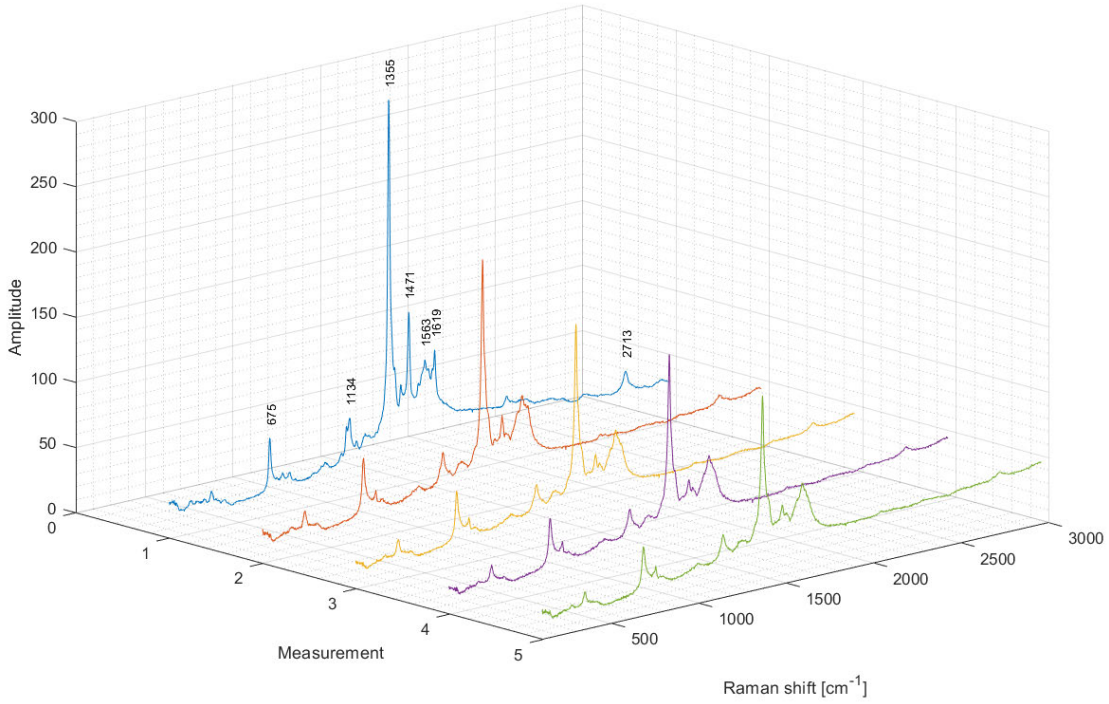

Figure 49: [20-10-2021] Raman spectrum of 5 consecutive measurements of an RBC. Indicated peak locations belong to measurement 1 in blue.

Figure 49 shows some other interesting trends. One thing that can be observed is that the overall amplitude decreases the more measurements are taken. The largest decrease is from the first to the second measurement. After which the signal decreases with the other measurements, albeit less than the initial step. In general most of the main peaks indicated stay visible in all 5 measurements: 675, 1134, 1355, 1471 and 2713 cm^{-1}. However, the peaks at 1563 and 1619 change quite drastically. In the first measurement in blue both peaks are still distinctly observable. In the succeeding measurements both peaks seem to vanish leaving a single peak at 1588 cm^{-1}. The 1471 cm^{-1} and the 1355 cm^{-1} peak are important in the determination of the oxidation state of the haemoglobin. The regression seen from the 1563 and 1619 cm^{-1} peaks in figure 49 might have to do with photophysics occurring during the first measurement. When the laser hits the haemoglobin molecules, a large portion of the light is absorbed. This can induce any trapped oxygen to be released (if there is any present) from the haemoglobin. It might also alter or destroy the haemoglobin molecules, causing a change in the Raman spectrum to occur.
The following experimental settings seem to work excellent to measure RBCs: 195 μW, 100 ms exposure time. This doesn't destroy the RBC and enables multiple measurements on the same cell. Accepting a lower signal in consecutive measurements.
In figure 48 the two RBCs shown have a higher (red) intensity in the middle of the cells. This is odd as a healthy RBC will have its flat disk shape with a thinner centre. Meaning that the concentration of haemoglobin should be higher on the edges. This shape can be seen in figure 47. To check if the cells are homogeneous a 4 cluster PCA analysis has been done, shown in figure 50.

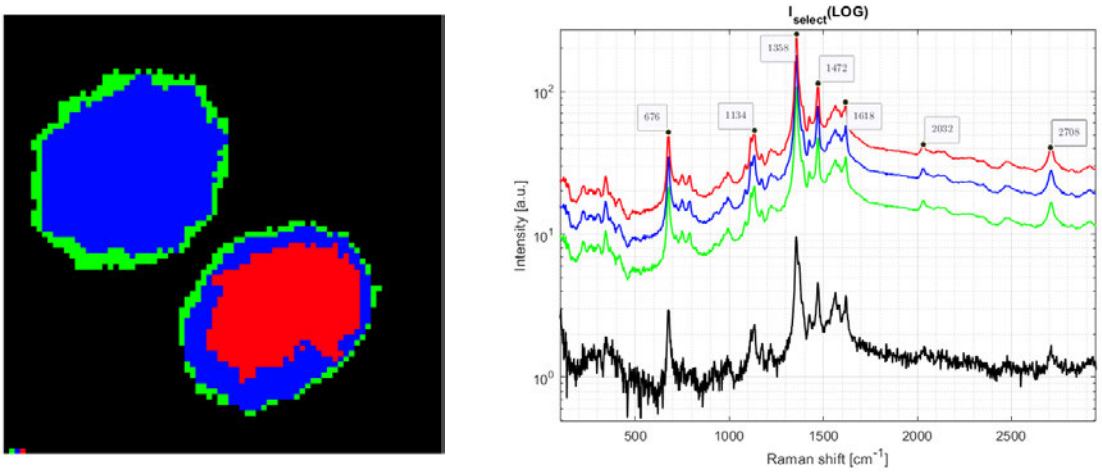

(a) (b)

Figure 50: [20-10-2021/output-7oct-2022] **(a)** 4 cluster PCA analysis of RBCs. **(b)** Logarithmic spectrum PCA analysis.

The cluster analysis shows a difference in intensity within the RBCs. With brighter centres and less bright edges. However, all three colours (red, blue and green) show the same spectral peaks. Meaning that a difference in homogeneity is unlikely. Another aspect is the RBC spectrum in the black background. Although the magnitude is an order of magnitude smaller, there still is some signal to be found. Cause of this signal could be destruction of RBCs during fixation or sample preparation. The broken down RBCs will float around in the background.

4.2.4 Oxygenation state

Raman spectroscopy can be used to determine the oxygenation state of haemoglobin, as shown by Almohammedi.[12] He imaged the different oxygenation states with multiple wavelengths, including 405nm. Comparing measurements should give an indication of the oxygenation state of our used RBCs. Figure 51a shows our measured RBC at 195 μW power, 100 ms exposure time, 18x18 μm ROI, 90x90 steps and 4 pixel box width average. Figure 51b shows Almohammedi's measurements at $\sim$ 300 μW power, 30s exposure time, a spatial resolution less than 1 μm, objective: Oil immersion Nikon 1.25NA 100X.

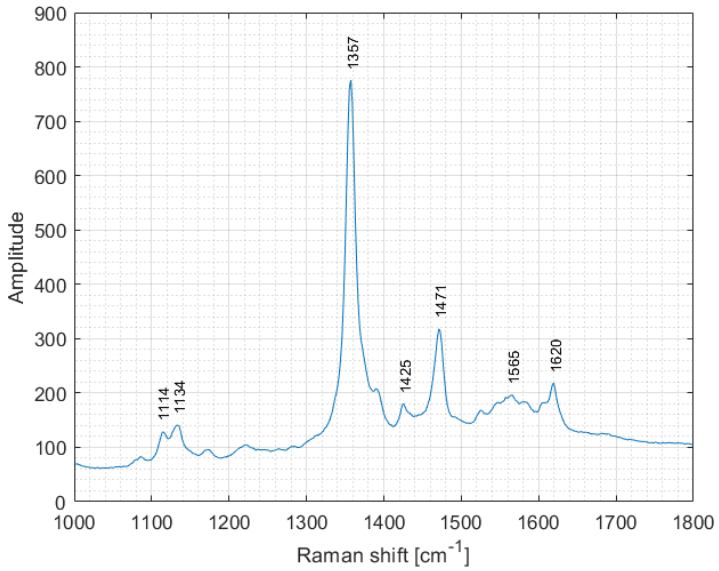

(a) [15-10-2021] 195 μW power, 100 ms exposure time, 18x18 μm ROI, 90x90 steps and 4 box width average.

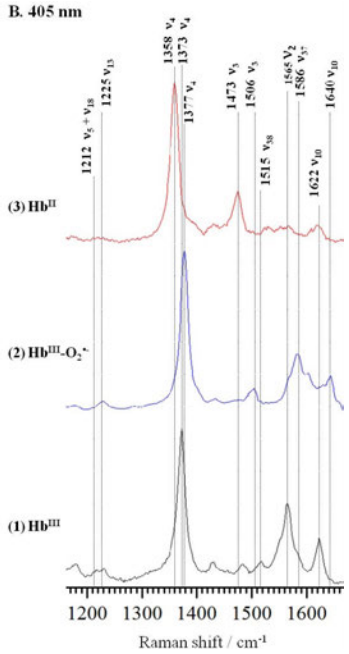

(b) $\sim$ 300 μW power, 30s exposure time, a spatial resolution less than 1 μm. (1) Methemoglobin. (2) Oxygenated Hb. (3) Deoxygenated Hb.[12]

Figure 51: Oxygenation state of RBCs

The main peak of figure 51a sits at 1357 cm^{-1}. Together with the second largest peak at 1471 the spectrum corresponds to the top graph in figure 51b. Meaning the measured RBCs are in their deoxygenated state. This can also be concluded when comparing the spectra in figure 51b with data from the article by Tsubaki et al.[13] They have measured both oxi- and deoxyhaemoglobin with a 406.7 nm laser. Where their three main peaks for deoxyhaemoglobin (1358, 1473 and 1622 cm^{-1}) overlap with the measured (1355, 1471 and 1619 cm^{-1}) peaks.

4.3 White Blood Cells

The next step in enzyme detection is the measurements on White Blood Cells (WBC). The power below the objective is increased compared to the RBC measurements (see section 5.2.2).

4.3.1 Cultured THP-1 cells

Cultured THP-1 cells are commonly used for enzyme analysis. Multiple measurements were performed to see if enzymes could be measured. Figure 52 shows the brightfield image of the imaged THP-1 cell with the red square indicating the scanned region. The cell was imaged using the following settings: 1.16 mW, 100 ms, 16x16 μm, 80x80 step size and 3 pixel box width average.

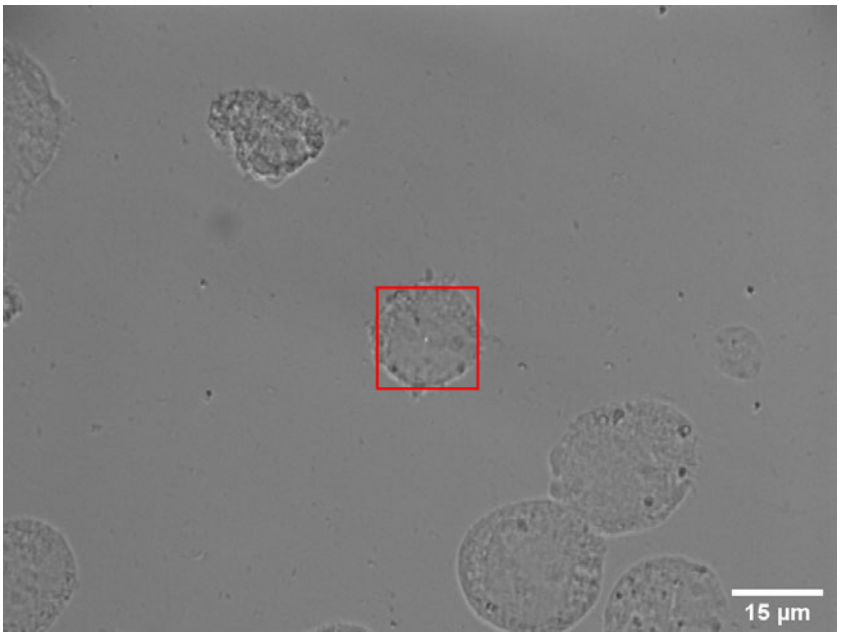

Figure 52: [30-11-2021, M11a] Brightfield image of THP-1 cell. Red square indicates scanned region.

Inside the QCR program cells are analysed at various point in the spectrum. This results in different locations for different peaks in the spectrum. This is shown in figures 53a and 53b. Figure 53a shows the locations of multiple objects with their peak around $2877cm^{-1}$. This shows from the spectrum in figure 53b. Another location and spectrum are shown in figures 54a and 54b. Here the main peak is chosen at $1362cm^{-1}$ (box width = 21). The last location and spectrum are shown in figures 55a and 55b. With the main peak chosen at $1667cm^{-1}$ (box width = 40).

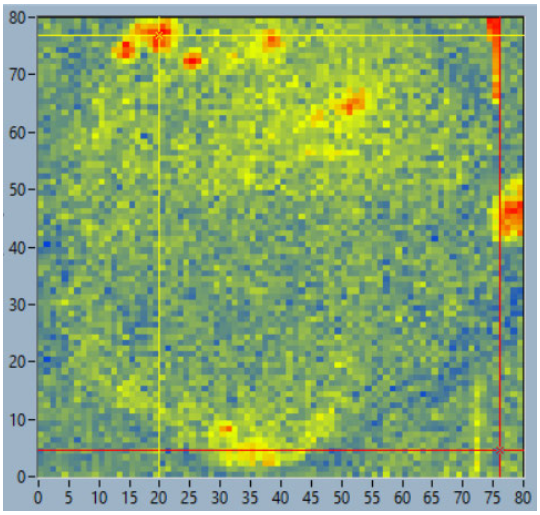

(a)

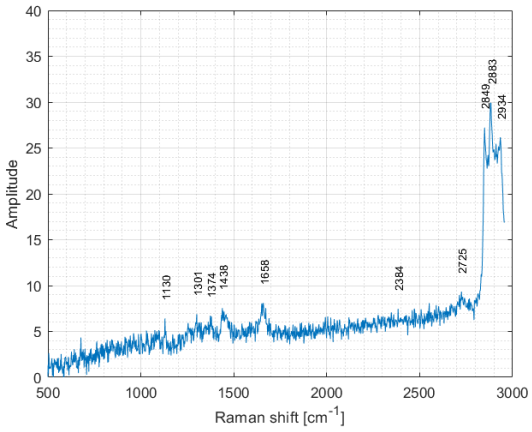

(b)

Figure 53: [30-11-2021, M11a] **(a)** THP-1 crosshair image at 2877 cm^{-1} (box width = 40).**(b)** Spectrum at yellow crosshair.

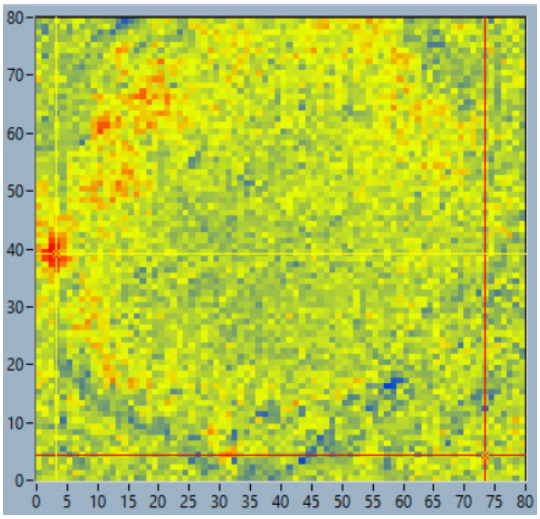

(a)

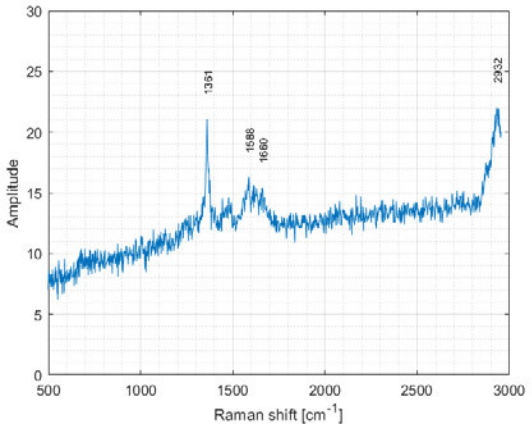

(b)

Figure 54: [30-11-2021, M11a] **(a)** THP-1 crosshair image at 1362 cm^{-1} (box width = 21).**(b)** Spectrum at yellow crosshair.

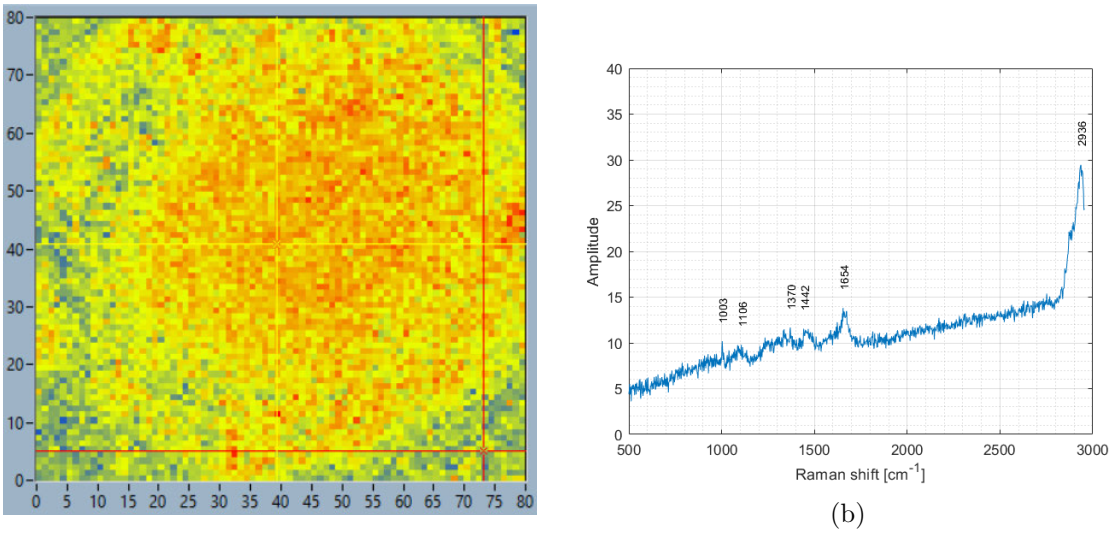

(a) (b)

Figure 55: [30-11-2021, M11a] **(a)** THP-1 crosshair image at 1667 cm^{-1} (box width = 40).**(b)** Spectrum at yellow crosshair.

The THP-1 cells described above show clear distinct regions. Looking at figure 53, a few spots light up when the spectrum is set at 2877 cm^{-1} (box width = 40 cm^{-1}). The main peaks present for these spots exist in the high Raman shift region (2800-3000), with peaks at 2849, 2883 and 2934 cm^{-1}. These peaks are associated with CH_2 (2849 and 2883) and CH_3 (2936) stretching.[10] These high intensity peaks in the high region are characteristic for lipid spectra.[14] As lipids are found all around a cell, the localisation of the red spot is somewhat odd. It might indicate a cluster of lipids or perhaps a few lipid droplets.
The spectra in figure 54 show a different image with more signal present in the 1300-2000 cm^{-1} region. The most distinctive peaks being 1361, 1588 and 1660. These peaks show up in research done by Sijtsema et al. as well. Their measurements with a 413.1 nm laser showed these peaks to associate with reduced cytochrome b_{558} and reduced meyeloperoxidase (MPO). Both molecules that are associated with interactions with the superoxide anion (O_2^-). They are also two molecules that can cause various diseases when lacking or absent.[15] The peak at 2932 cm^{-1} indicates the presence of lipids which are of course abundant throughout the cell.
Finally, in figure 55, some other peaks appear as well. The 1003 peak, for instance, is associated with the protein phenylalanine.[16] And 1654 is associated with Amide I or a double bonded carbon atom (C=C).[17]

Using PCA (Principle Component Analysis) it is also possible to assign different regions to a cell as described in section 3.5. Figure 56a shows the result of the THP-1 cell divided in 7 clusters. The corresponding spectra are shown in figure 56b.

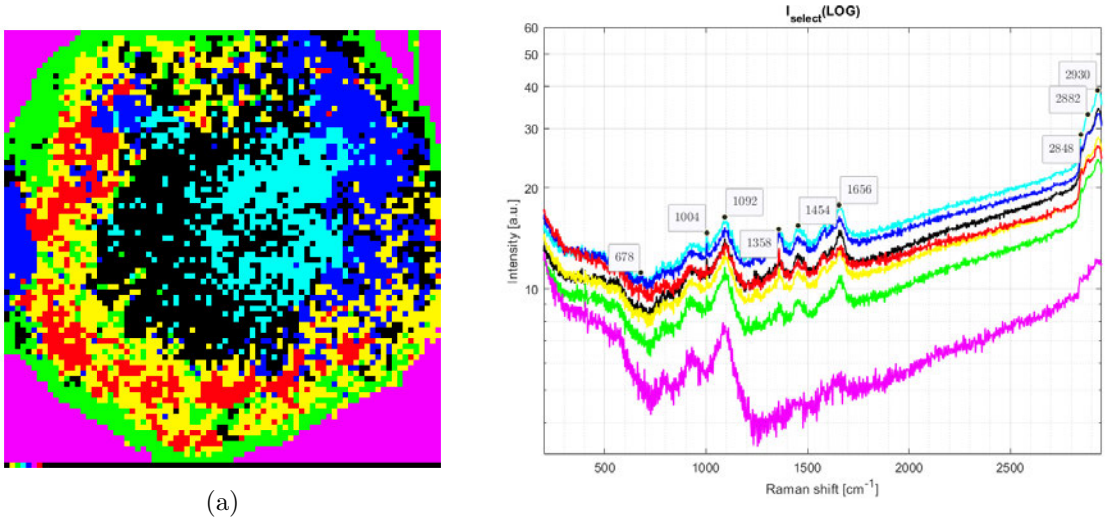

(a) (b)

Figure 56: [30-11-2021/output-10-May-2022, M11a] **(a)** THP-1 PCA analysis for 7 clusters.**(b)** Logarithmic spectra of 7 clusters.

Some of the different regions can be found in the cluster analysis of figure 56. Most of the aforementioned peaks appear in the PCA giving off some distinct regions. However, there still is quite some overlap from the regions. Apart from the purple background, the coloured pixels from different regions are still quite scattered within the cell.

4.3.2 Donor sample WBCs

A blood donor sample was used as a more realistic sample compared to the cultured THP-1 cells. The sample was prepared as described in section 3.3 to obtain White Blood Cells for analysis. Figure 57 shows a brightfield image of three WBC's and the scanned region indicated by the red square. The cells were scanned at 2.004 mW, 100 ms exposure time, 80x80 steps at 16x16 um and 3 pixel box width average.
Analysis with the QCR program gives the results shown in figures 58a and 58b. Here the spectrum was analysed at 1452 cm^{-1}. The same cells were also analysed with PCA using 5 clusters to divide the cell. The results are shown in figures 59a and 59b.
Figures 58 and 59 show similar results to the HTP-1 cell. Some peaks are clearly distinguishable from the background (1004, 1440 and 1660 cm^{-1}). Cellular components stand out from the light blue background but it is somewhat hard to identify different cell components.

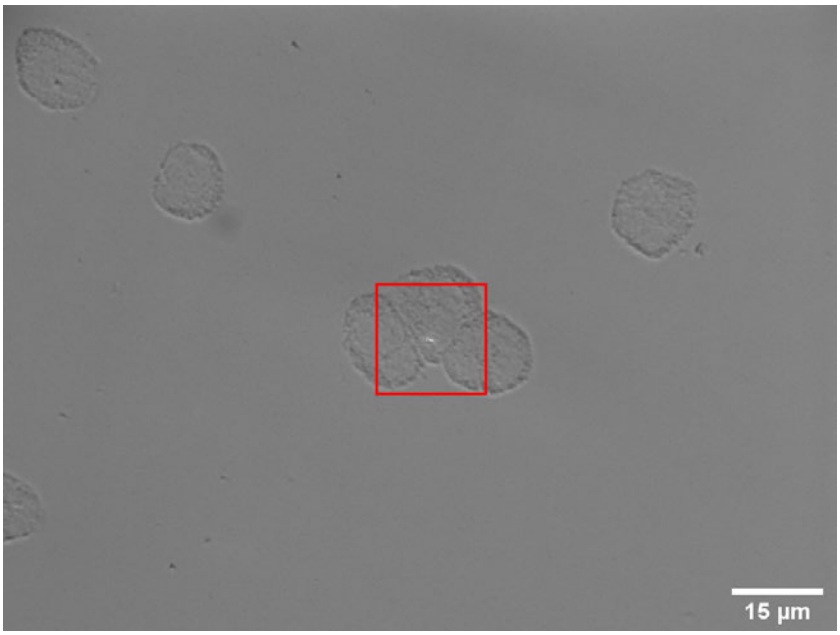

Figure 57: [09-11-2021/M3a-after] Brightfield image of three white blood cells. Red square indicates scanned region.

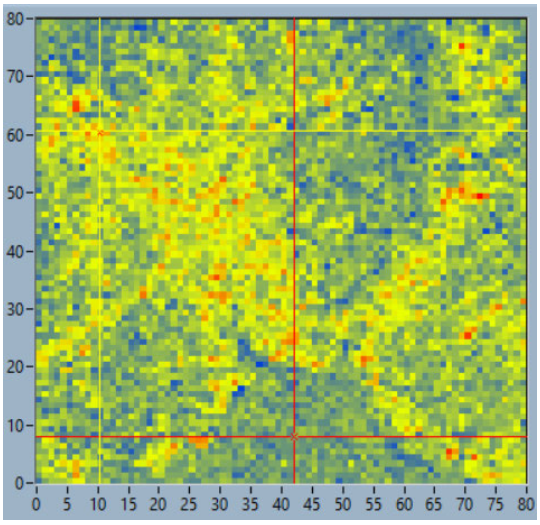

(a)

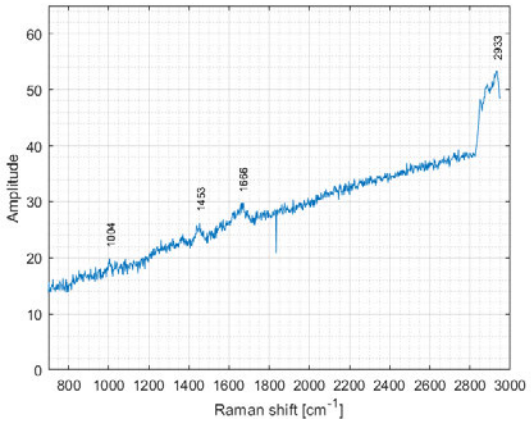

(b)

Figure 58: [09-11-2021] **(a)** Donor WBC crosshair image at 1452 cm^{-1} (box width = 30).**(b)** Spectrum at yellow crosshair.

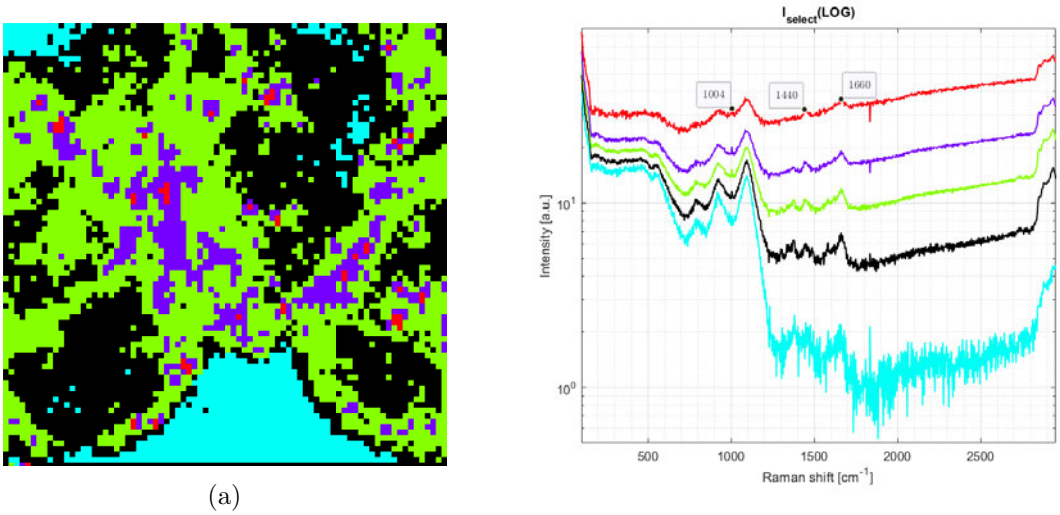

(a)

(b)

Figure 59: [09-11-2021/output-10-May-2022, WBC-pca-5] **(a)** Donor WBC PCA analysis for 5 clusters.**(b)** Logarithmic spectra of 5 clusters.

4.4 Other applications

4.4.1 Crystal detection inside synovial fluid

As a side project synovial fluid from a patient's knee was scanned to find crystals associated with gout. Using the polarisation filters the birefringent crystals can be spotted. In figures 61, 63 and 64 different materials have been successfully scanned.

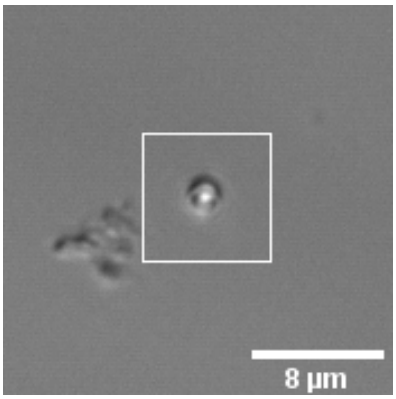

Figure 60: [30-11-2021, M14b-S4-after] 8x8μm, 40x40 steps, 1.16mW input, 200ms. Brightfield image of a Maltese cross in synovial fluid from a patient. White square indicates scanned region.

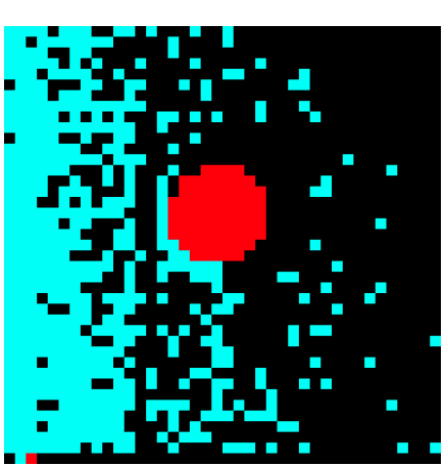

(a)

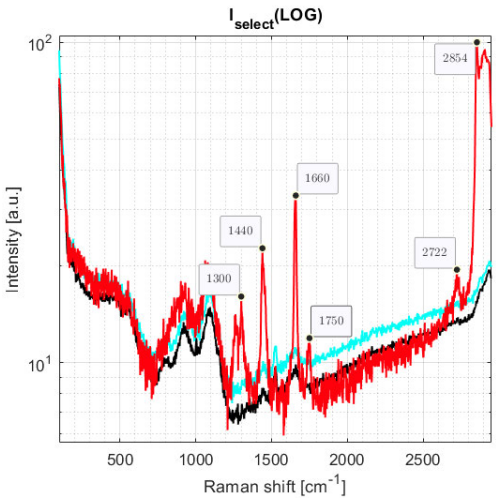

(b)

Figure 61: [30-11-2021, M14b] **(a)** Patient synovial fluid Maltese cross PCA analysis for 3 clusters.**(b)** Logarithmic spectra of 3 clusters.

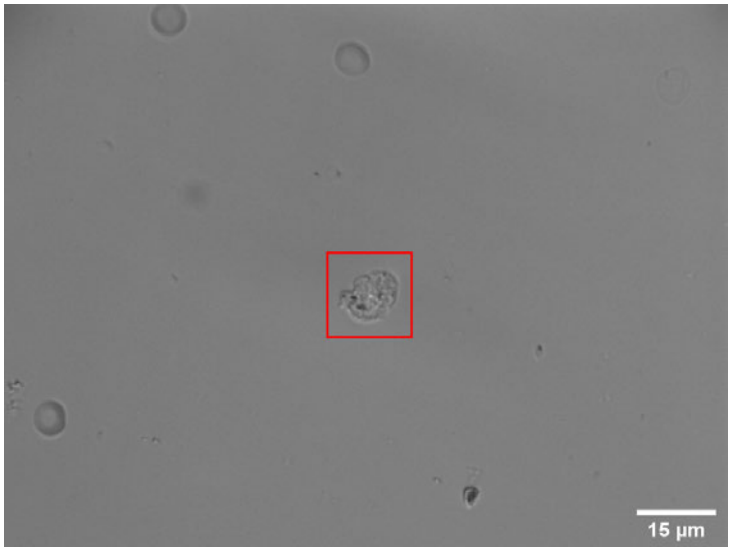

Figure 62: [30-11-2021, M9b-S2-after] 14x14μm, 70x70 steps, 1.16μW, 100ms. Bright-field image of a white blood cell in synovial fluid from a patient. Red square indicates scanned region.

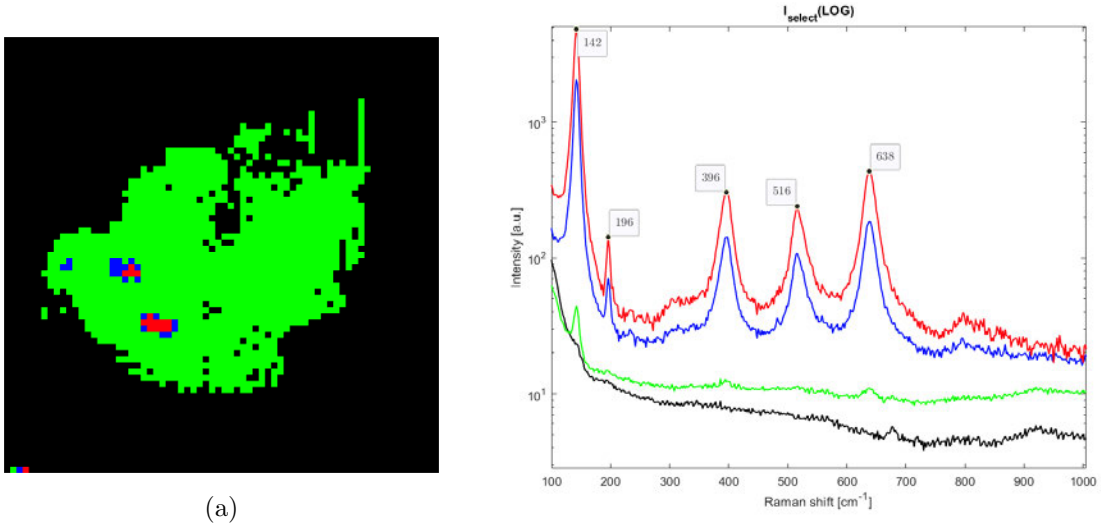

(a)

(b)

Figure 63: [30-11-2021, M9b-TiO] **(a)** Patient synovial fluid WBC PCA analysis for 4 clusters.**(b)** Logarithmic spectra of 4 clusters.[18]

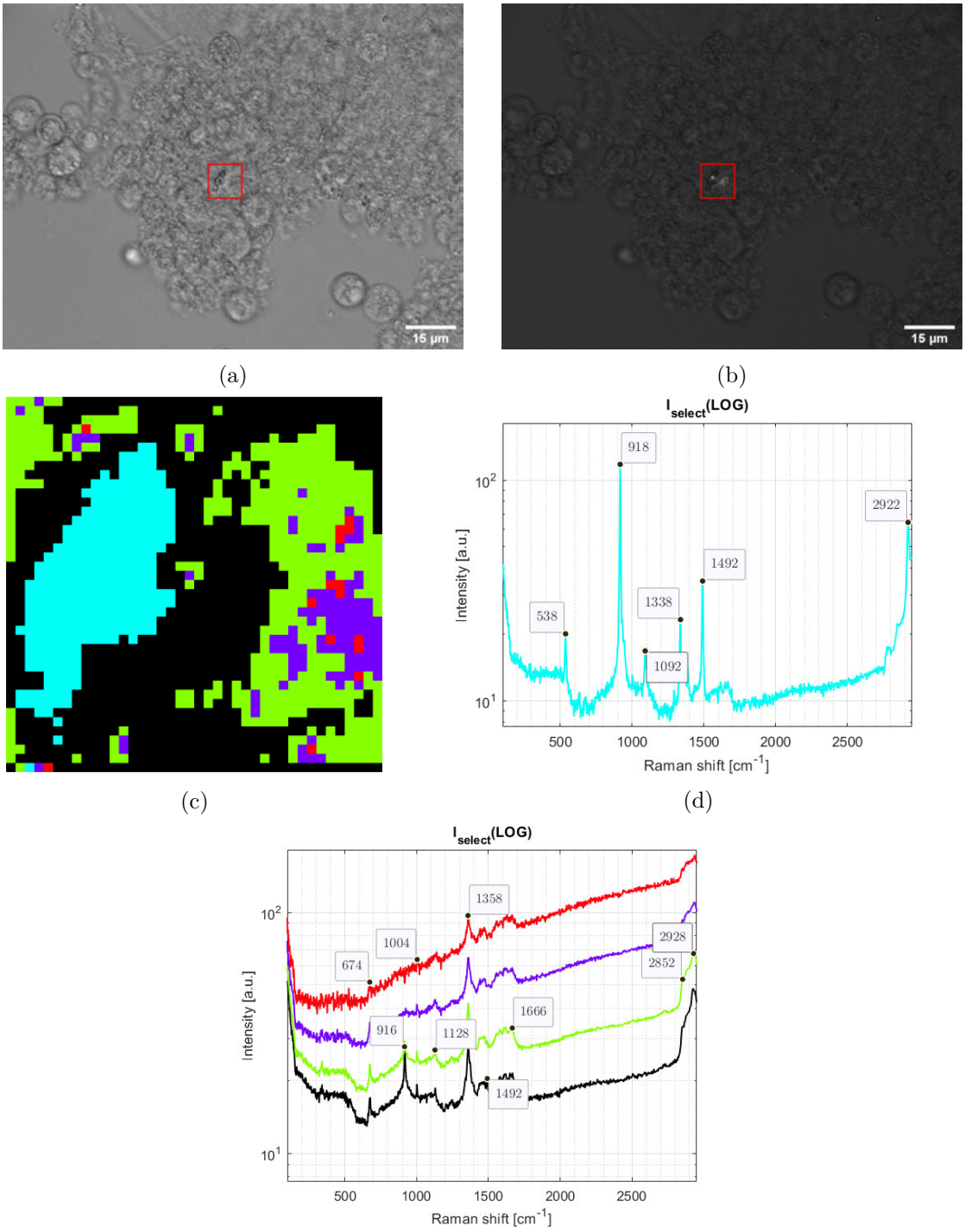

Figure 64: [22-11-2021, M7] 8x8μm, 40x40 steps, 1.16μW, 100ms.**(a)** Brightfield image of crystal.**(b)** Polarisation image of crystal.**(c)** PCA analysis with 5 clusters.**(d)** Light blue cluster spectrum.**(e)** Other cluster spectra.

5 Discussion

5.1 Setup

In the sections below only a few components from the setup are discussed. Either because they can be improved, or some additional comments needed to be made about the components. Components that are not further described have been deemed 'working as intended'. Table 2 shows which components are working, discussed or need to be improved.

Table 2: Overview of all components in the setup and if they are working, need improvement and whether or not they are discussed

Component	**Works as intended**	**Discussed in text**	**Needs improvement**
Laser	-	x	x
Shutter & Trigger	x	-	-
Laser cleanup filter	x	-	-
Polariser	x	-	-
Beam expander	x	x	x
407 nm razor edge	x	-	-
XYZ stage	x	x	x/-
Objective	x	-	-
40x40 um stage	x	-	-
Transmission light	x	-	-
Slide holder	x	-	-
Polarisation filters	x	x	x/-
CCD camera	x	x	-
Fidgets	x	-	-
Blue calibration LED	x	-	-
Krypton lamp	x	-	-
405 nm long pass	x	-	-
Prism box	x	-	-
Pinhole focus lens	x	x	-
Spectroscope	x	-	-

5.1.1 Laser

The laser has shown a multitude of unwanted behaviour during both the construction of the setup and the experimental phase. Starting with the instability when used with the optical fiber. When the optical fiber was removed the stability improved significantly with the added bonus of no power losses due to the fiber. Hence it was decided to keep using the laser without the optical fiber. Further investigation will be needed to determine the exact cause of this laser instability with the optical fiber. The power output and input are not yet fully reliable. This makes that the power always needs to be measured below the objective before a measurement. It also means that it is difficult to estimate what the power will be based on the input power. How the laser output behaves over the entire power spectrum will need to be investigated further.

5.1.2 Beam expander

Together with inspection of the laser the beam expander will need to be improved in the future such that it more closely fits the opening of the objective and improves the resolution of the image. This means changing the lenses for the appropriate magnification.

5.1.3 XYZ stage

The XYZ stage works as intended for the most part. Where the X and Y direction are easily controlled by the joystick, the Z direction can be slow and tedious. The large knob requires many revelations to go from a position where the power can be measured, to a position where a sample can be analysed. The Z knob does not contain an upper limit, making it possible to press the sample into the objective. With possible damage to either sample or objective as a result. When moving the XY stage with the joystick the total movement in either direction is limited as well. When moved too far the stage will catch the condenser, resulting is possible bending or damage of the condenser.
To ensure damage prevention in the future, a solution for these limits can be investigated.

5.1.4 Polarisation filters

The polarisation filters work as intended as birefringent objects are easily detected. However, the quality of the polarisation filter below the microscope glass can be improved in the future. This might result in clearer birefringent images and improve detection even more. Another improvement could be the positioning of the polarisation filter. It's now attached to the cover slide which means that too much movement with the XY stage results in additional movement of the slide to align the filter below the sample.

5.1.5 CCD camera

The CCD camera works as intended. One issue in the protocol of experiments is that the camera image needs to be horizontally flipped at the start of the day. This is done in the CCD camera software and if forgotten, the CCD image and the spectroscope image will be mirror images. In the future a better solution for this might be found.

5.1.6 Pinhole focus lens

The pinhole focus lens works as intended for the most part. One problem encountered is that during some calibrations the magnitude of the measured signal from the spectroscope is less than expected. Twisting the X and Y knobs of the pinhole focus lens improves the magnitude of the signal again. It is unknown why the alignment might change over time and this is something which needs further investigation.

5.2 Cells and other objects

5.2.1 RBC

The red blood cells are easily detected with the 405 nm setup. However, further research needs to investigate after how many consecutive measurements the cell's signal completely drops off or when the cell is too damaged. Furthermore, additional investigation is needed to find the cause of the Raman shifts in the regression experiment.

5.2.2 WBC

Early measurements on White blood cells (WBCs) with similar measurement conditions (0.195 μW, 40ms) to RBCs yielded very little result. This might have to do with the very high concentration of porphyrin molecules in haemoglobin. WBCs don't have these high concentrations and might need higher powers in order to detect the molecules of interest. More suitable measuring conditions will need to be found.

5.2.3 THP-1

The THP-1 cells show potential for the detection of different regions, but there is still quite some overlap present. This might be improved with further research into optimal measuring conditions. The appearance of all the different peaks does prove that the 405 nm setup is capable of detecting different cellular components.

5.2.4 Donor sample WBC

To compare the results of the cultured THP-1 cell line, measurements were performed on a WBC from a donor. Similar peaks were found in both the WBC's and the THP-1 cells. But as with the THP-1 cells, the cell components are not very distinguishable and overlap. Meaning that better suited measurement settings need to be found.

5.2.5 Other applications

Alongside the measurement of cells the 405 nm setup proved very useful in other applications as well. Figures 60 and 61 show that the signal from a Maltese cross (a type of lipid droplet) is overwhelming with distinct peaks at 1300, 1440, 1660, 1750, 1722 and 2854 cm^{-1}. Minamikawa et al. found similar peaks with excitation of a 532 nm laser.[19] This proves that identification of lipid droplets only several micrometers in size is possible with the 405 nm setup. Potentially being used to identify lipid droplets in for instance liver samples. Tackling research into non-alcoholic fatty liver disease (NAFLD).
The other useful application is the identification of metallic structures inside cells. Figures 62 and 63 show results of our published discovery of titanium dioxide (anatase) inside a white blood cell. Taken from synovial fluid of a patient with a swollen ankle joint. The anatase signal is magnitudes of degrees higher than the background signal. Proving the use of the 405 nm setup in the detection of materials/metals that are not body's own. These materials can be sub micrometer and still be picked up easily by the Raman setup.
Lastly the 405 nm setup can be used to identify crystalline structures inside cells or surrounded by cells from a patient. The polarisation filters help in the search for these birefringent crystals. The birefringent objects are easily noticed by their bright spots on the CCD camera. This is shown in figure 64b. After locating an object of interest the scanning shows the distinctive peaks of the crystal as shown in figure 64d. The cells in the background don't pose any difficulty in detection of the crystal as the signal stands out from the others. As of now this crystal's identity is unknown as a matching peak pattern has not been found yet. Indicating that there is still much to be found/investigated inside patient samples that has not been identified yet.

6 Conclusion

6.1 405 nm setup

Construction of the 405 nm setup has been an all-round success. Many of the components are working as intended. With a regular Raman setup introduction, new users are able to operate the setup within a few days. Many components are already automated and don't require any user inputs. There are some components that still need to improved though. Most prominently the 405 nm laser. As described in both sections 2.2 and 5.1.1 the laser shows some undesired behaviour. For better future usability of the setup the laser will need to be sent to the manufacturer for a checkup. The same applies to the optical fiber. When the laser has a more stable power output the light shining on the cells will be more equal, meaning every component of the cell will have the same power input. A renewed laser should fix the problem of the non-Gaussian beam as well. Fixing this problem allows for the beam expander to be set correctly to the opening size of the objective. Filling the entire opening and improving resolution at the sample.
The XYZ stage works as intended but could improve on usability and safety precautions to limit sample damage. Similarly the polarisation filters work as intended but especially the bottom filter below the sample can be improved. This would make detection of birefringent objects even easier.
The pinhole focus lens drift is something which needs to be looked into further. Either this lens itself drifts or some other component in the setup might twist/turn/relax over time. Changing the light path very slightly.

6.2 Experiments

The toluene calibration measurements prove the power of the 405 nm setup compared to the 647 nm. Needing 3.5 times less power to obtain 1.6 times more signal. The 405 nm setup is an excellent setup to detect any molecules containing Soret bands, making use of the power of resonant Raman. Disadvantage is that only a few resonant modes are observed a great deal and some of the smaller modes will be lost in the background. Making distinction of different cellular components harder.
The setup is able to easily detect the oxygenation state of red blood cells. Further research is required to determine the exact cause of Raman shifts during consecutive measurements.
Measurements on the white blood cells proved a good start but require a good deal of further research as well. Investigation into suitable laser powers and exposure times is something which should be prioritised.
Results on the other applications of the setup are very promising. In all three categories (lipids, metals and crystals) the setup showed very clear measurements which made identification of the material at hand quite simple.

7 Acknowledgements

I would really like to thank Aufried Lenferink for his daily assistance, guidance and knowledge in the construction of the 405 nm setup. It wouldn't be possible without your help. I would also like to thank my supervisor, Cees Otto for his guidance, support and empathy throughout the entire project. I would like to thank Leon Terstappen, Armağan Koçer and Nienke Bosschaart for their feedback and participating as committee members.
I wish to show my appreciation to the staff and fellow students of the MCBP group at the University of Twente for their assistance and provided help. A special thanks goes to Tom Niessink, with whom I had the pleasure to publish our article. Also thanking him for his useful writing feedback in the final construction of this thesis.
Finally I would like to thank my friends, family and roommates for their unconditional support and lending an ear whenever needed.

A Appendix

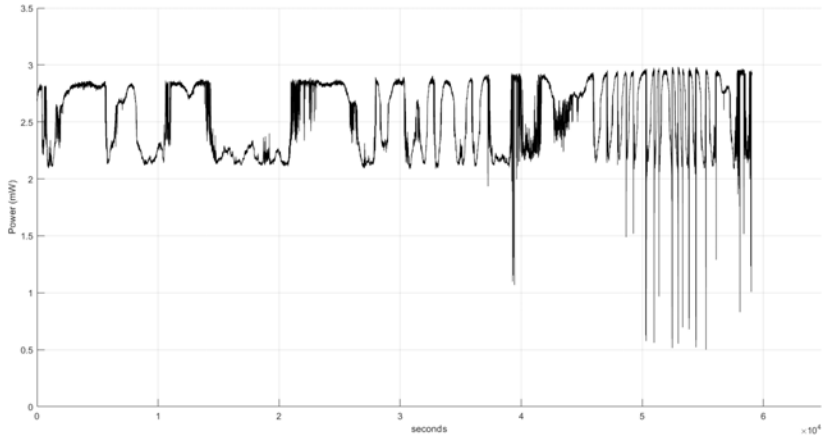

Figure 65: [10-6-2021] 18 hour measurement of laser with optical fibre encoupled. Input at 5mW.

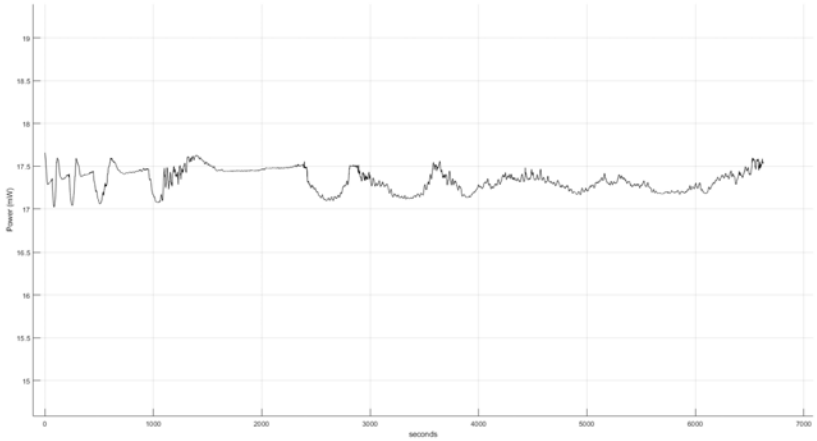

Figure 66: [15-6-2021] 2 hour measurement of laser with optical fibre encoupled. Input at 40mW.

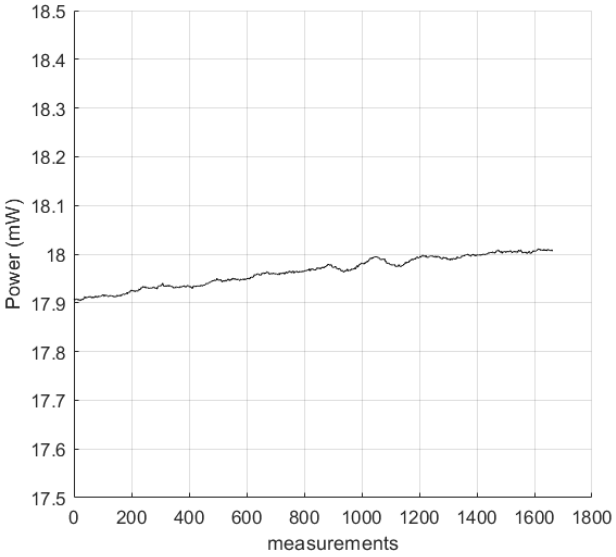

Figure 67: [08-06-2021] 5 min measurement of laser without optical fibre encoupled. Input at 20mW.

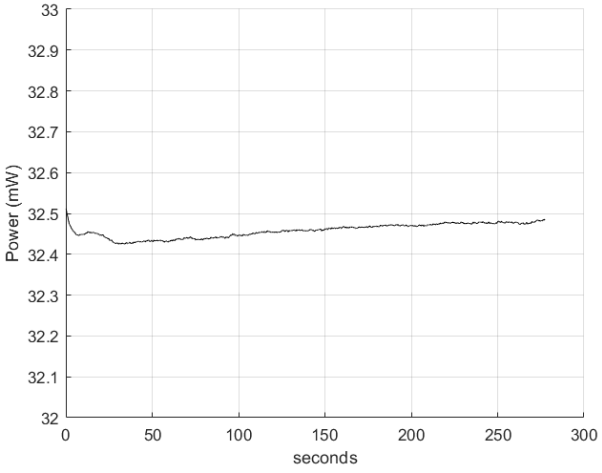

Figure 68: [08-06-2021] 5 min measurement of laser without optical fibre encoupled. Input at 40mW.

A.1 Matlab script for asc file analysis

```
clear; close all; clc;

spec_raw = 'with_cleanup.txt';
% back = 'back_405.txt';
spec = table2cell(readtable(spec_raw,'Delimiter','tab', ...
    'ReadVariableNames', false));
% Tback = table2cell(readtable(back,'Delimiter','tab', ...
%   'ReadVariableNames',false));

x = str2double(spec(:,1))/10^9;
y = str2double(spec(:,2))/10^9;

%% Plot other graphs
% spec_raw2 = 'bleach2.txt';
% spec_raw3 = 'bleach3.txt';
% spec_raw4 = 'bleach4.txt';
% spec_raw5 = 'bleach5.txt';
%
% spec2 = table2cell(readtable(spec_raw2,'Delimiter','tab', ...
%   'ReadVariableNames',false));
% spec3 = table2cell(readtable(spec_raw3,'Delimiter','tab', ...
%   'ReadVariableNames',false));
% spec4 = table2cell(readtable(spec_raw4,'Delimiter','tab', ...
%   'ReadVariableNames',false));
% spec5 = table2cell(readtable(spec_raw5,'Delimiter','tab', ...
%   'ReadVariableNames',false));
%
% x2 = str2double(spec2(:,1))/10^9;
% y2 = str2double(spec2(:,2))/10^9;
% x3 = str2double(spec3(:,1))/10^9;
% y3 = str2double(spec3(:,2))/10^9;
% x4 = str2double(spec4(:,1))/10^9;
% y4 = str2double(spec4(:,2))/10^9;
% x5 = str2double(spec5(:,1))/10^9;
% y5 = str2double(spec5(:,2))/10^9;

%%

% yback = str2double(Tback(:,2))/10^9;
% y_tol = y - yback;
x_left = 0;
x_right = 1600;
lin_type = '-';
z = ones(1,1600);
figure(1);
p = plot(x,y,lin_type)
set(gca, 'YScale', 'log')
% p = plot3(x,z,y,lin_type);
xlabel('Pixels');
% xlabel('Pixels')
```

```
ylabel('Counts');
% ylabel('Measurement')
% ylabel('Wavelength (\lambda)');
axis([x_left x_right 0 1000]);
% title('Haemoglobin spectrum')

%% Plot other graphs
% hold on
% z2 = z*2;
% p2 = plot3(x2,z2,y2,lin_type);
% hold on
% z3 = z*3;
% p3 = plot3(x3,z3,y3,lin_type);
% hold on
% z4 = z*4;
% p4 = plot3(x4,z4,y4,lin_type);
% hold on
% z5 = z*5;
% p5 = plot3(x5,z5,y5,lin_type);
% set(gca, 'YDir','reverse')
%%
%[pks, locs, w, p] = findpeaks(y,x,"MinPeakProminence",3500,
% "MinPeakHeight",5.4,"MinPeakDistance",0);
%indices = find(locs<100);
% locs(indices) = [];
% pks(indices) = [];
%str = string(round(locs));
% z_h = ones(length(locs),1);
% loc_axis = locs>x_left;
% prom = p>2;
% out = loc_axis.*prom;
% locs = locs(loc_axis);
% pks = pks(loc_axis);
% str = str(loc_axis);
% h = text(locs,pks+2000,str,'FontSize',8);
% % h = text(locs,z_h,pks+10,str,'FontSize',8);
% set(h,'Rotation',90);
grid on;
grid minor;
%%
% ax = gca;
% exportgraphics(ax,'Heamoglobin_spectrum.png','Resolution',600)
```

A.2 Matlab script for spectroscope calibration file analysis

```
clear; close all; clc;
spec_raw = 'ALL_cal.txt';

spec = table2cell(readtable(spec_raw,'Delimiter','tab', ...
    'ReadVariableNames',false));

x = str2double(spec(2:end,1))/10^6; % Pixels
y = str2double(spec(2:end,2))/10^6; % wavelength
z = str2double(spec(2:end,3))/10^6; % cm-1
r = str2double(spec(2:end,4))/10^6; % rel. cm-1
q = str2double(spec(2:end,6))/10^6; % rel. cm-1

res_lambda = (max(y)-min(y))/1600;
res_cm = (max(z)-min(z))/1600;

lin_type = '-';
p = plot(y,q,lin_type);
% set(gca, 'ydir', 'reverse')
axis([404 465 0 70000]);
% ylabel('\lambda (nm)');
% ylabel('cm{^-1}')
ylabel('Quantum Efficiency')
% ylabel('rel. cm{^-1}')
% xlabel('Pixels');
xlabel('Wavelength (\lambda)')
% xlabel('Raman shift (cm^{-1})')
grid on;
grid minor;
```

Bibliography

[1] Van Manen HJ, Van Bruggen R, Roos D, Otto C. Single-cell optical imaging of the phagocyte NADPH oxidase. Antioxidants and Redox Signaling. 2006;8(9-10).

[2] Nitzan M, Romem A, Koppel R. Pulse oximetry: Fundamentals and technology update; 2014.

[3] Carey P. Biochemical Applications of Raman and Resonance Raman Spectroscopes. Elsevier; 1982.

[4] Tu Q, Chang C. Diagnostic applications of Raman spectroscopy; 2012.

[5] Vanna R, Ronchi P, Lenferink ATM, Tresoldi C, Morasso C, Mehn D, et al. Label-free imaging and identification of typical cells of acute myeloid leukaemia and myelodysplastic syndrome by Raman microspectroscopy. Analyst. 2015;140(4).

[6] Dorosz A, Grosicki M, Dybas J, Matuszyk E, Rodewald M, Meyer T, et al. Eosinophils and Neutrophils-Molecular Differences Revealed by Spontaneous Raman, CARS and Fluorescence Microscopy. Cells. 2020;9(9).

[7] Lee MW, Lee DL, Yen WN, Yeh CY. Synthesis, optical and photovoltaic properties of porphyrin dyes. Journal of Macromolecular Science, Part A: Pure and Applied Chemistry. 2009;46(7).

[8] Josefsen LB, Boyle RW. Photodynamic therapy and the development of metal-based photosensitisers; 2008.

[9] Van Manen HJ, Uzunbajakava N, Van Bruggen R, Roos D, Otto C. Resonance Raman imaging of the NADPH oxidase subunit cytochrome b 558 in single neutrophilic granulocytes. Journal of the American Chemical Society. 2003;125(40).

[10] Krafft C, Knetschke T, Funk RHW, Salzer R. Identification of organelles and vesicles in single cells by Raman microspectroscopic mapping. In: Vibrational Spectroscopy. vol. 38; 2005. .

[11] Olympus. UPLXAPO40X;. Available from: `https://www.olympus-lifescience.com/en/objective-finder/#!objective=511710235`.

[12] Almohammedi AR. Direct Measurements of Heme Concentration in Heart Cells by Raman Spectroscopy; 2016.

[13] Tsubaki M, Srivastava RB, Yu NT. Resonance Raman Investigation of Carbon Monoxide Bonding in (Carbon monoxy)hemoglobin and -myoglobin: Detection of Fe-CO Stretching and Fe-C-O Bending Vibrations and Influence of the Quaternary Structure Change. Biochemistry. 1982;21(6).

[14] Czamara K, Majzner K, Pacia MZ, Kochan K, Kaczor A, Baranska M. Raman spectroscopy of lipids: A review; 2015.

[15] Sijtsema NM, Otto C, Segers-Nolten GMJ, Verhoeven AJ, Greve J. Resonance Raman microspectroscopy of myeloperoxidase and cytochrome b558 in human neutrophilic granulocytes. Biophysical Journal. 1998;74(6).

[16] Schie IW, Huser T. Methods and applications of Raman microspectroscopy to single-cell analysis. In: Applied Spectroscopy. vol. 67; 2013. .

[17] Matthews Q, Jirasek A, Lum J, Duan X, Brolo AG. Variability in Raman spectra of single human tumor cells cultured in vitro: Correlation with cell cycle and culture confluency. In: Applied Spectroscopy. vol. 64; 2010. .

[18] Niessink T, Ringoot J, Otto C, Janssen M, Jansen TL. Clinical Images: Detection of titanium dioxide particles by Raman spectroscopy in synovial fluid from a swollen ankle. Arthritis & Rheumatology. 2022.

[19] Minamikawa T, Ichimura-Shimizu M, Takanari H, Morimoto Y, Shiomi R, Tanioka H, et al. Molecular imaging analysis of microvesicular and macrovesicular lipid droplets in non-alcoholic fatty liver disease by Raman microscopy. Scientific Reports. 2020;10(1).